IOWA STATE UNIVERSITY
Digital Repository

Retrospective Theses and Dissertations

Iowa State University Capstones, Theses and Dissertations

1-1-2002

Investigation of the phase formation and magnetic properties of the Fe-N thin films deposited by reactive pulsed laser deposition

Nanlin Wang
Iowa State University

Follow this and additional works at: https://lib.dr.iastate.edu/rtd

Recommended Citation

Wang, Nanlin, "Investigation of the phase formation and magnetic properties of the Fe-N thin films deposited by reactive pulsed laser deposition" (2002). *Retrospective Theses and Dissertations*. 21351.
https://lib.dr.iastate.edu/rtd/21351

This Thesis is brought to you for free and open access by the Iowa State University Capstones, Theses and Dissertations at Iowa State University Digital Repository. It has been accepted for inclusion in Retrospective Theses and Dissertations by an authorized administrator of Iowa State University Digital Repository. For more information, please contact digirep@iastate.edu.

Investigation of the phase formation and magnetic properties of the Fe-N thin films deposited by reactive pulsed laser deposition

by

Nanlin Wang

A thesis submitted to the graduate faculty
in partial fulfillment of the requirements for the degree of
MASTER OF SCIENCE

Major: Materials Science and Engineering

Program of Study Committee:
John E. Snyder, Co-major Professor
Alan P. Constant, Co-major Professor
Vikram L. Dalal

Iowa State University
Ames, Iowa
2002

Copyright © Nanlin Wang, 2002. All rights reserved.

Graduate College
Iowa State University

This is to certify that the master's thesis of

Nanlin Wang

has met the thesis requirements of Iowa State University

Signatures have been redacted for privacy

TABLE OF CONTENTS

ACKNOWLEDGMENTS

First of all, I would like to express my sincerest appreciation to my major professors, Dr. John E. Snyder and Dr. Alan P. Constant, who gave me such a great opportunity to join the research group in Ames Laboratory and the Microelectronics Research Center, and provided such an interesting research area for me. From them, I learned not only the methods and knowledge, but also the attitude for doing research, i.e. hard working and insisting on the truth. I cannot be more grateful to their guidance and help and encouragement throughout all my research work and study.

Secondly, I would like to extend my sincerest appreciation to Dr. Chester C. H. Lo. I cannot thank more for his kind help and his warm encouragement.

Also, I am grateful to Prof. V. K. Pecharsky for illuminating discussions, and appreciate the help of Mr. J. L. Harringa and Dr. B. A. Cook in XRD measurements.

Last, I'd like to thank all the members in our magnetics group of Ames Laboratory. Their thoughts, cooperation, and friendship are really appreciated.

ABSTRACT

Fe-N films have been grown on SiO_2/Si(100) substrates by reactive pulsed laser deposition (PLD). Series of films were deposited at 20°C and at 250°C, with a wide range of nitrogen pressures. Nitrogen pressure was found to affect film average composition, structure, phase percentages, and magnetic properties of the films. Deposition temperature also affected the nitrogen content, structure, phase percentages and magnetic properties of the films. The saturation magnetization of the films is shown to depend not only on their average nitrogen content but also on the phases and their relative amounts that make up the films. In particular, the iron nitrides γ'-Fe_4N, and ε-Fe_3N (which has a wide range of composition) play a major role in determining the magnetization. Results can be understood in terms of the relative contributions of deposition rate and atomic surface diffusion in producing thin-film structure. To date, no giant moments larger than M_s of pure Fe have been observed in this investigation.

Subsequently annealing at 200°C shows that for the sample deposited at 10mTorr and 20°C the perpendicular magnetic anisotropy is suppressed after annealing. This can be understood by the explanation that the annealing process releases the stress. For the sample deposited at 40mTorr and 20°C (which is amorphous or possibly nanocrystalline), after annealing its magnetization is found to decrease significantly. This may be due to the reason that annealing makes the distribution of the introduced nitrogen atoms more homogeneous (or ordered). N nearest neighbors are proposed to tend to decrease the moments on Fe atoms, and thus it is assumed that spreading the N more homogeneously could cause more iron atoms to have N neighbors and thus overall moment to decrease.

1. LITERATURE REVIEW

1.1 The Fe-N Phase Information.

Since 1972 when Kim and Takahashi [1,2] reported that they discovered a new magnetic material of α''-$Fe_{16}N_2$ compound with the highest saturation magnetization of about 2200 emu/cm^3 (3.0μ_B/Fe) which is larger than that of 35% Co-65% Fe (2.5μ_B/Fe), α''-$Fe_{16}N_2$ has become one of the most interesting materials in the field of magnetism. This is due to the chaotic situation that scientists cannot make sure whether its giant magnetic moment is true or not since its discovery in 1972. The Kim and Takahashi discovery in 1972 made a strong impact on the research fields of magnetic materials and magnetism. After that, many research groups have been interested in this material and have tried to identify its magnetism. However, experimentally proposed values of magnetic moment in α''-$Fe_{16}N_2$ vary widely from 1710 emu/cm^3 (equal to pure iron) to 2500 emu/cm^3 (larger than 35% Co-65% Fe) [3]. Therefore many researchers began to wonder if "one is looking at the revolutionary results or egregious errors [4]"[5,6].

The phase information of the Fe-N system for bulk materials is shown in Fig. 1-1.[7] The equilibrium solid phases of the condensed Fe-N system according to the phase diagram are [7]: (1) the terminal bcc solid solution denoted as ferrite or α-Fe; (2) the terminal fcc solid solution denoted as austensite or γ-Fe; (3) the fcc nitride, Fe_4N or γ', with a narrow range of composition near 20 at.% N; (4) the cph nitride, ε-Fe_3N, with a broad range of composition from about 15 to at least 33 at.% N; and (5) the orthorhombic nitride, Fe_2N or ζ, with a composition ranging from about 33 at. % N to an unknown upper limit. There are

also two kinds of nonequilibrium phases that have been observed which are: (1) bct Fe-N martensite or α', and (2) the ordered bct nitride, $Fe_{16}N_2$ or α''.

If nitrogen gas or mixtures of NH_3 and H_2 are passed over Fe powder or thin films at elevated temperatures, several kinds of nitrides form. One of these is γ-FeN, the nitrogen austenite where Fe is in a fcc arrangement and N randomly occupies some of the octahedral interstices. As the nitrogen content increases, the nitrogens interact and at high concentrations γ'-Fe_4N forms. In γ'- Fe_4N (Fig1-2.), the iron is in a fcc arrangement and the nitrogens occupy the octahedral interstices in an ordered manner.

When the γ-FeN formed at elevated temperatures is slowly cooled, it decomposes into the mixture of α-Fe (or α-Fe with a small amount of N in solid solution) and γ'-Fe_4N. However, if it is quenched to room temperature or below, the phase transformation into α-Fe and Fe_4N is suppressed and the α' martensite forms. If α'-FeN is then heat treated at temperatures between 120 and 150°C, ordering of the nitrogens can occur and a new phase forms, which is α''-$Fe_{16}N_2$ (Fig.1-2). It is tetragonal and the unit cell dimensions are roughly double those of the α' phase [8].

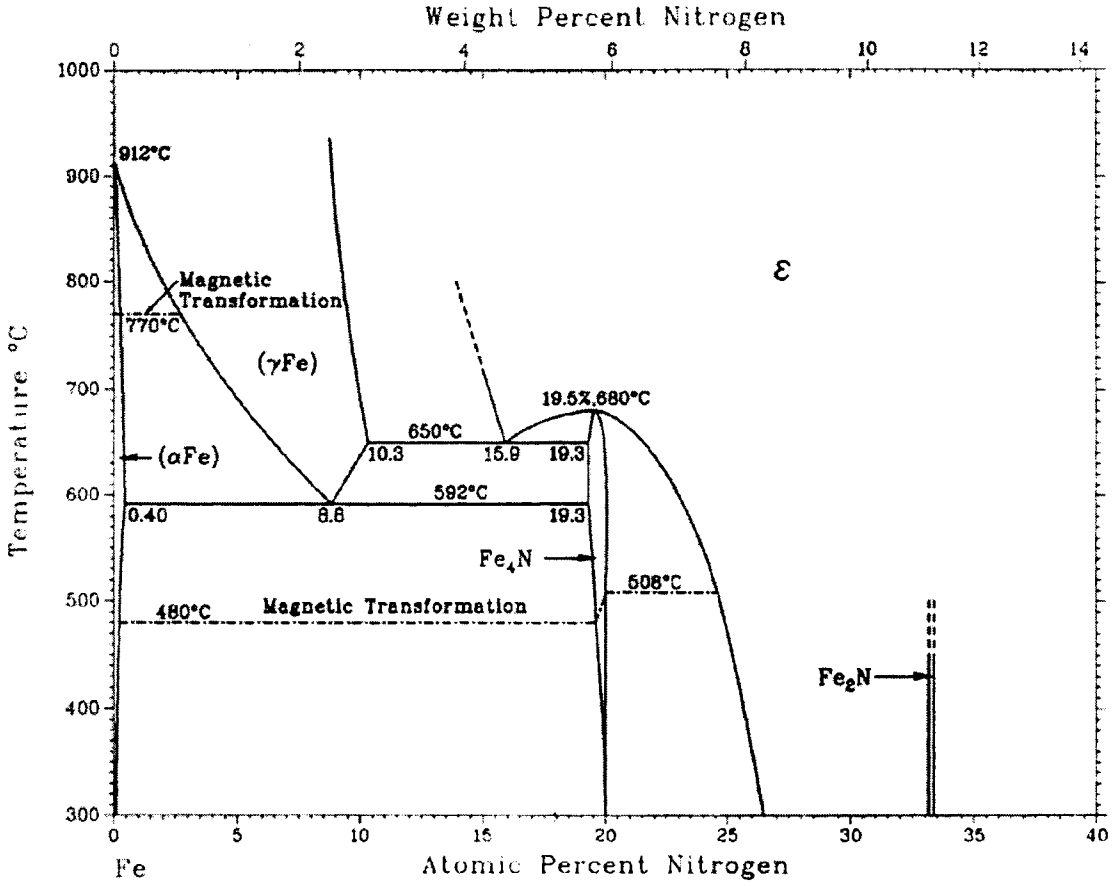

Figure1-1 The phase information of Fe-N system [7]

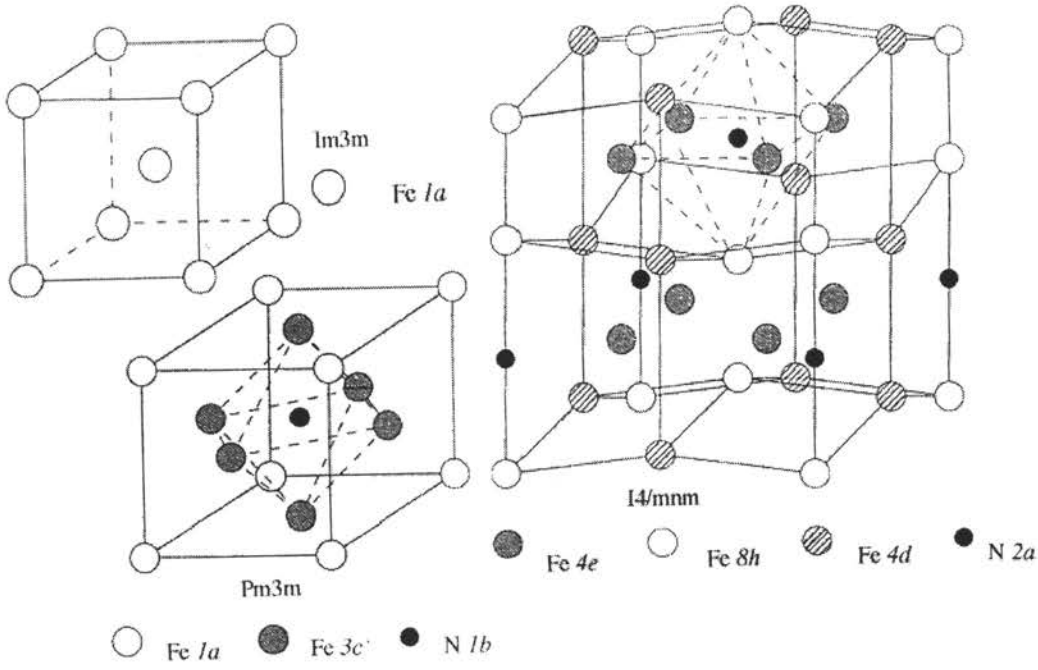

Figure1-2 Crystal structures of α-Fe, γ'-Fe_4N and α''-$Fe_{16}N_2$, drawn to scale [9].

1.2 The Previous Studies about Fe-N Thin Films.

In order to fabricate the material or phase of α''-$Fe_{16}N_2$, various methods have been applied. Among them are reactive sputtering [10], ion beam assisted deposition (IBAD)[11], molecular beam epitaxy (MBE)[12], and ion implantation [13].

Among the works that stand for the high magnetization of α''-$Fe_{16}N_2$, Okamoto et al. [14] reported that epitaxial Fe-N films have been grown on Fe or Ag (001) single-crystal underlayers by the sputter beam method. On both underlayers the Fe-N films were observed to have a bct structure (α'-martensite). Postannealing was reported to promote ordering of nitrogen atoms in the bct lattice and this resulted in precipitation of a metastable α''-$Fe_{16}N_2$ phase in Fe-N films. Based on XRD and RHEED, the formation of α''-$Fe_{16}N_2$ was clearly observed in the films annealed at 200°C, and the magnetization of the annealed Fe-N films tended to increase with increasing the volume fraction of the α''-$Fe_{16}N_2$. They also studied the effect of lattice distortion on the magnetic and electronic state of α''-$Fe_{16}N_2$ [15]. In that research, they also fabricated epitaxial (α''+α')-$Fe_{16}N_2$ films on Ag (001) underlayers by sputter beam method. It was found that with the decrease of the film thickness, the unit cell volume of α''-$Fe_{16}N_2$ increased and a giant magnetic moment up to 2.8 μ_B/Fe atom was found (the atomic magnetic moments for pure Fe are 2.2μ_B/Fe). Moreover, with increase of the unit cell volume, the X-ray diffraction intensity ratio $I_{\alpha''(002)}/I_{\alpha''(006)}$ was apparently decreased. From their theoretical calculations, reduction of $I_{\alpha''(002)}/I_{\alpha''(006)}$ means increase of the valency of N atoms in α''-$Fe_{16}N_2$. So the authors thought that the charge transfer from N to Fe due to lattice expansion effect results in the increase of the magnetic moment of α''-$Fe_{16}N_2$.

Using ion-beam-assisted deposition, Jiang et al [16] deposited Fe-N films with a higher magnetization (237 emu g^{-1}) than that of bulk Fe (210 emu g^{-1}). During the post annealing, the $Fe_{16}N_2$ was stable at 150°C and began to decompose into α-Fe and γ'-Fe_4N at 200°C. After annealing at 300°C for 2h the $Fe_{16}N_2$ transformed completely to α-Fe and γ'-Fe_4N. Moreover, although the M_s-value of the Fe-N film containing $Fe_{16}N_2$ is significantly higher than that of α-Fe, the M_s of $Fe_{16}N_2$ seems less than that reported by Kim and Takahashi [1]. So the authors suggested a more accurate measurement of the percent of $Fe_{16}N_2$ in the film is necessary to determine its M_s-value.

Ding et al [17] found that they did get increased magnetization moment (as high as 230 emu g^{-1}) larger than that of pure iron (210 emu g^{-1}) among their Fe-N thin films through a reactive ion beam sputtering deposition method. However, they think that these high magnetization values are attributed to the presence of nitrogen in the iron sublattice, rather than the α'/α'' phase directly.

Up to now, the highest magnetization of Fe-N thin films was reported by Sugita et al. [3]. They reported a magnetization of 2500 emu/cm^3 for a single-phase, single-crystal $Fe_{16}N_2$ film epitaxially grown by MBE on the GaAs (001) substrate. The experiment was conducted by evaporating Fe in an atmosphere of mixed gas of N_2 and NH_3, following by annealing. During deposition, the substrate temperature was 200°C. It was found that without annealing, only Fe-N martensite peak was identified. After an annealing procedure under 200°C for 90h, the X-ray showed that the Fe-N martensite completely changed into α''-$Fe_{16}N_2$.

In the voices against the high magnetization of α''-$Fe_{16}N_2$, Takahashi and Shoji found that although they produced the α''-$Fe_{16}N_2$ by reactive sputtering, they did not observe a

magnetization as high as that of the Hitachi group [18]. They reviewed the literature of α″-$Fe_{16}N_2$ films with and without giant magnetic moment in connection with structure and magnetic moment. It was found that the results of XRD and TEM analysis did not show any difference between α″-$Fe_{16}N_2$ films with and without giant magnetic moment. However, the Mössbauer spectrum was quite different in each case. The hyperfine field of $Fe_{16}N_2$ film synthesized by themselves splits into three hyperfine field interactions, but for an $Fe_{16}N_2$ film with giant magnetic moment fabricated by the Hitachi group the hyperfine field interaction did not split and is almost the same as that of pure α-Fe. Thus Takahashi and Shoji believe that the interaction of Mössbauer spectra is the key item to solve the α″-$Fe_{16}N_2$ problem.

Being a Mössbauer spectroscopist, J.M.Cadogan [19] proposed his opinion after studying the Mössbauer results. In his opinion, α″-$Fe_{16}N_2$ does not have a giant magnetic moment on the Fe atom, although it is closer to strong ferromagnetism than α-Fe and one of the Fe sites in the α″-$Fe_{16}N_2$ structure does have a larger magnetic moment than α-Fe. In this article, the author also reviewed several theory calculation results based on band theory. It seems that all of these results stand in the *against* camp.

There are also other evidences against large moments, which come from foils [20], large particles [20], some sputtered films [6], theoretical study [21] and so on.

The argument is focused on two aspects [18]: First whether or not the proposed giant magnetization values larger than that of 35%-65% Co-Fe are accurate, since it is difficult to derive M_s from measurements on very thin films and very difficult to determine volume fractions of multiphase thin films. Second, if the values are accurate, whether or not they are due to α″-$Fe_{16}N_2$. α″-$Fe_{16}N_2$ phase is difficult to identify, and there is no reliable method for

determining the volume fraction of α''-$Fe_{16}N_2$ in thin films. Furthermore there is insufficient data on M_s for other Fe nitrides present in multiphase samples (some have wide ranges of composition).

Although there are different opinions on the large moments being associated with α''-$Fe_{16}N_2$, it is important and interesting for researchers to study it. Because if there are giant moments in Fe-N, such values of magnetization cannot be explained on the basis of the Slater-Pauling curve and challenge the current theoretical models of magnetism.

PLD (pulsed laser deposition) is a recent, efficient and economical method to fabricate thin films. Only one group has previously reported results on Fe-N films deposited by reactive pulsed laser deposition (PLD) [22]. In Coey's review paper [9], the author concluded that the common features of many of the reports claiming giant magnetization values are: reduced dimensionality of the samples (i.e. very thin films, very fine powders, multiphase nanostructures) or strained structures (i.e. epitaxial films, strained multiphase nanostructures) or both. Compared with these common features, Yoshitake and Ohkoshi's results have several quite unusual features. First, they report a film average M_s as high as 2300 emu/cm^3 for films 200 to 500 nm thick (much thicker than most other reports), and deposited onto glass substrates (which are amorphous substrates, hence no epitaxial effects). Furthermore, they do not propose that the elevated moments are due to the ordered α''-$Fe_{16}N_2$ (which they did not observe), but rather, speculate that the increased saturation magnetization was due to a heterogeneous state of γ'-Fe_4N precursors within an α^*-phase (a new phase which they propose, with a bct structure with lattice constants a = 0.285 nm and c = 0.287 nm). However, composition measurements are not reported, which makes phase identification difficult.

In the present work, using pulsed laser deposition, we want to answer the following questions:

1) What is the effect of substrate temperature and nitrogen pressure on the phase formation and magnetic properties of the Fe-N thin films?

2) Can we observe the high magnetization of Fe-N thin films reported by T. Yoshitake and M. Ohkoshi's group?

2. EXPERIMENTAL METHODS AND PROCEDURES

2.1 Overview of Pulsed Laser Deposition [23]

Pulsed laser deposition (PLD) is one of the simplest and most versatile thin film growth techniques. It uses laser radiation as an external energy source to vaporize materials and deposit thin films in vacuum or predetermined background atmosphere. One of its important advantages is that PLD is a non-equilibrium process that allows for the reproduction of stoichiometry from the target to the film. The other is extremely high instantaneous growth rates.

There are various kinds of laser types used in PLD systems including excimer, Nd-YAG, and $TEACO_2$. Among them, excimer lasers are commonly ones that emit radiation directly in the UV range.

The light output from an excimer laser evolves from a molecular gain medium where the lasing action occurs between a bound upper electronic state and a repulsive or weakly bound ground state. Because the ground state is repulsive, the excimer molecule can dissociate rapidly ($\sim 10^{-13}$s) as it emits a photon during transition from upper state to ground state.

The deposition process of PLD system is shown in Fig.2-1. The laser beam is directed through an aperture, passes through a focusing lens and the laser window, and then into the vacuum chamber and finally hits the target. Consequently, highly energetic ions and atoms are ejected from the target as the result of laser-target interaction. The incoming beam is at 45° with respect to the normal of the target. The substrate is parallel to the target about 7cm

away. During deposition, the target keeps rotating, which makes the deposition uniform. Singh and Kumar have classified the PLD process into four separate regimes [24].

1. Interaction of the laser beam with the target resulting in ablation of surface layers.
2. Interaction of the ablated materials with the incident laser beam resulting in isothermal plasma formation and expansion.
3. Anisotropic adiabatic expansion of the plasma in the direction of the substrate.
4. Interaction of the plasma with the background gas.

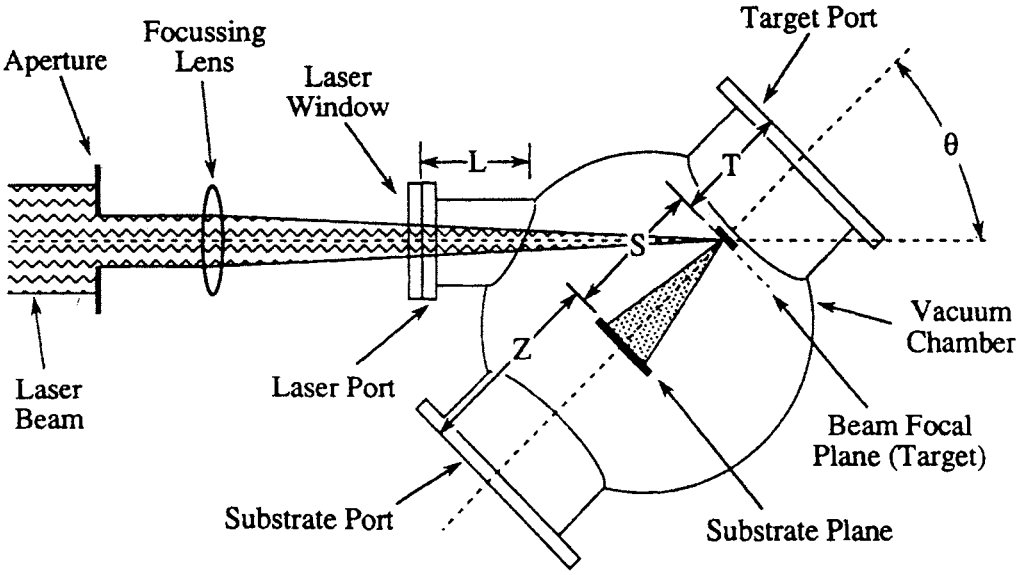

Figure 2-1 Schematic illustration of the deposition process of the PLD system [23].

For a PLD system, there are several important process parameters, which include substrate temperature, background gas pressure, pulse energy density, pulse repetition rate, target-substrate distance, and focal length. Among them, the substrate temperature and background gas pressure are usually changed for experimental purposes, and others are fixed for a given material. Energy density can be adjusted by either changing the pulse energy or the distance between the focal lens and target. Very high energy density can increase the speed of the ejection and deposition of particles onto the substrate, and help the formation of metastable structures in the film. Finally, a shorter distance between the substrate and the target may allow for faster deposition rates. A background gas is introduced into the chamber to provide the atomic and molecular precursors that are required to produce a desired film composition. Ionization of the background gas takes place due to the interaction of the ablated material plume with the background gas and also the further interaction between the plume, background gas, and subsequent laser pulses. The pressure of the background gas can change the growth parameters such as the deposition rate, spatial distribution, and kinetic energy distribution of the depositing species. As pointed out by Chrisey and Hubler, there are four direct results on the plasma plume due to raising the background gas pressures [23].

1. A decrease of the deposition rate due to the increase of collisions.
2. A sharpening of the plume boundary, indicative of a shock front
3. A slowing of the plume relative to the propagation in vacuum
4. Spatial confinement of the plume.

The deposition system used in this investigation is a turbo-pumped Neocera PLD system with a typical base pressure of 8×10^{-7} Torr. The laser was a Kr-F eximer laser (248 nm wavelength). The laser energy was 200 mJ with pulse duration less than 50 ns. The power density at the target was ~3.5 W/cm^2 and repetition rate of the laser pulse was 10 Hz. The target used during the deposition process was a 99.99% Fe.

2.2 Vibrating Sample Magnetometer [25]

The vibrating sample magnetometer (VSM) measures magnetic properties of materials. When a material with a magnetic moment is made to undergo sinusoidal motion (i.e. mechanically vibrated), it produces a periodic magnetic flux change at the location of adjacent pick-up coils. This induces a periodic electrical signal in the pick-up coils, whose amplitude is proportional to the magnetic moment of the sample.

However, the induced signal is also proportional to the vibration amplitude and frequency. Therefore a servo system is introduced to maintain the vibration amplitude and frequency. This technique depends on feedback from a vibrating capacitor, one of whose plates moves with the sample holder assembly, located beneath the transducer to generate an ac control signal that varies solely with the vibration amplitude and frequency. This signal is fed back to the oscillator where it is compared with the drive signal so as to maintain constant drive output. It is also phase-adjusted (to ensure there is no relative phase-shift with respect to the induced signal from the pick-up coils) and routed to the signal demodulator (which is located in the lock-in amplifier) where it functions as the reference drive signal.

A lock-in amplifier is used to measure the amplitude and phase of signals buried in noise. In the lock-in amplifier, a demodulator operates by multiplying the induced signal in

the pickup coils and the reference signal from the vibrating capacitor. Since there is no relative phase-shift between the induced signal and reference signal, the demodulator output takes the form of a sinusoid at twice the reference frequency, but with a positive mean level. This process is shown in Fig. 2-2 [26].

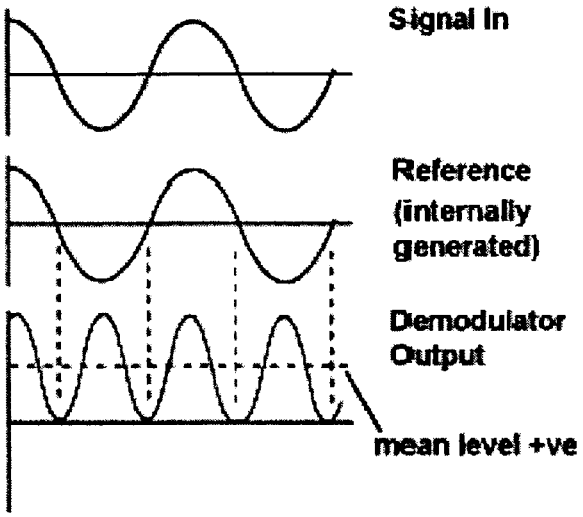

Figure 2-2. The illustration of the output of the demodulator in the lock-in amplifier [26].

If the reference signal amplitude is maintained, then by measuring the mean level, the amplitude of the input signal (i.e. induced signal) can be determined. To get the mean level, it is a relatively simple task to isolate it by using a low-pass filter which is set to a sufficiently low cut-off frequency. The noise which has no fixed frequency or phase relationship to the reference, is also multiplied by the reference signal in the demodulator, but does not result in any change to the mean level. Therefore it is rejected by the low-pass filter, and the resulting signal is an analog of the moment magnitude of the sample alone.

During measurement, by slowly varying the applied magnetic field (generated by an electomagnet with soft magnetic pole pieces), a hysteresis loop indicating the dependence of the sample's total magnetic moment on the external applied magnetic field is therefore measured.

In the present work, the VSM used is the Model 4500 manufactured by EG&G Princeton Applied Research Corporation, and it was controlled from a PC by DOS software from Lakeshore, Inc. The maximum applied magnetic field is ± 7400 Oersted, and the vibrating frequency is approximately 82 HZ.

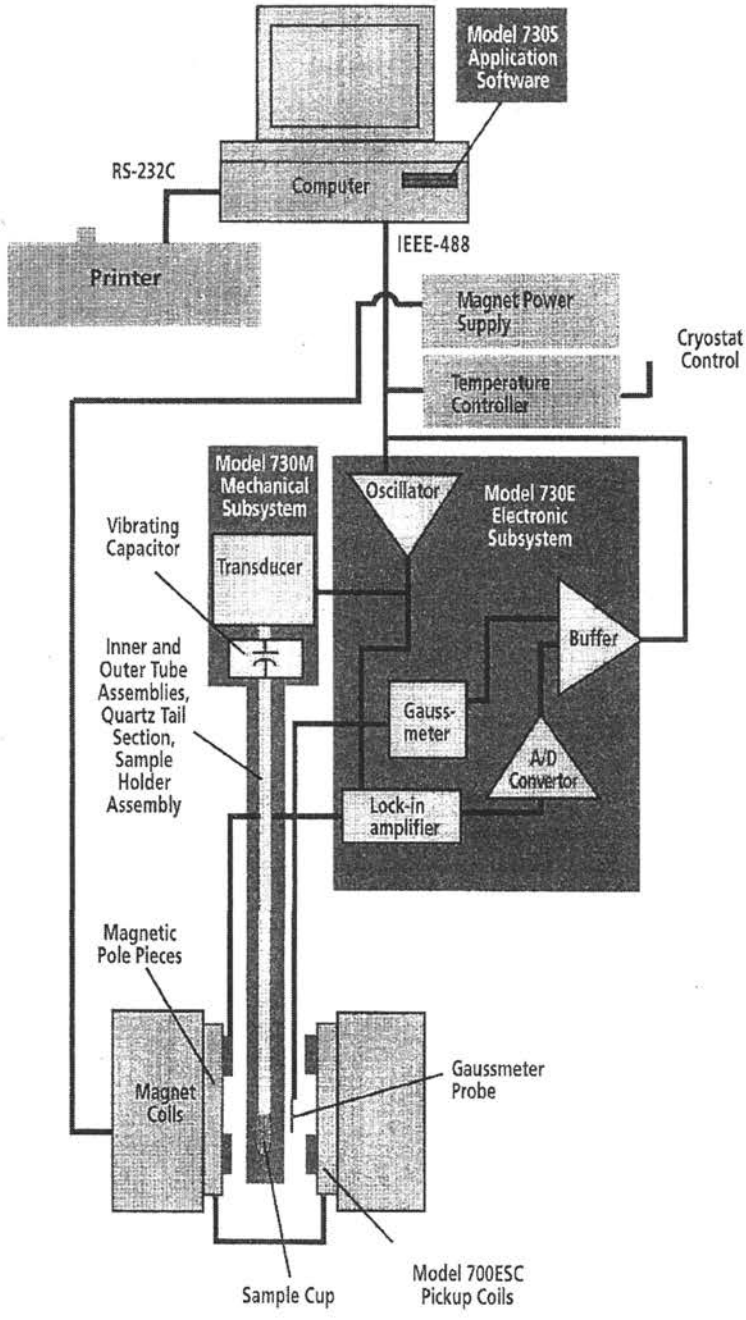

Figure 2-3 Schematic diagram of a vibrating sample magnetometer [25].

2.3 X-ray Photoelectron Spectroscopy [27]

X-ray photoelectron spectroscopy (XPS) was used to measure the atomic content of the nitrogen introduced into the iron nitride films as well as the content of other elements such as oxygen and carbon during deposition.

When a sample is irradiated by X-rays, photoelectrons are emitted. Photoelectrons can be generated from valence or inner electron levels depending on the energy of the X-rays. The ejected photoelectrons are focused by an electromagnetic lens system and gathered by an energy analyzer. The energy analyzer sweeps over an energy range and counts the number of electrons at each energy. This energy is really the electron binding energy, and according to the Einstein equation, it is given

$$E_B = h\nu - E_k - \phi$$

Where E_B is the binging energy, $h\nu$ is the X-ray energy, E_k is the photoelectron kinetic energy, and ϕ is the work function.

From the binding energy of photoelectrons, the energy state from which they were emitted can be characterized, which allows for the elemental characterization of the sample surface. However, the analysis depth of a typical XPS scan is limited to approximately the top 5 nm below the surface. Depth profiling can be done by combining the XPS analysis with an ion etch process.

In the current experiment, the measurements were performed using a Physical Electronics (PHI™) 5500 Multitechnique ESCA system with monochromatic Al K_α radiation. Depth profiles were determined by ion etching the sample surface using 4 kV Ar ions at 3μA total target current. Composition measurements were determined after sputtering through the surface oxide layer, and obtaining a nitrogen percentage stable with sputtering

time (typically after sputtering for 20 minutes, which corresponded to the removal of approximately 20 nm of surface film).

2.4 X-ray Diffraction [28]

X-rays are electromagetic radiation with very short wavelength (about 10^{-10}m), and they occupy the region between gamma and ultraviolet rays in the complete electromagnetic spectrum. X-rays are produced when any electrically charged particle of sufficient kinetic energy is rapidly decelerated.

The most fundamental principle of X-ray diffraction theory is the Bragg Law. Shown as in Fig.2-4, for example, two incident rays are scattered by atoms in two different planes. Therefore the path difference between these two rays is $2d\sin\theta$. The essential condition which must be met if diffraction is to occur is that these two scattered rays will be completely in phase. Thus the path difference must be equal to a whole number n of wavelengths, i.e.

$$2d\sin\theta = n\lambda$$

This is relation is known as the Bragg law.

Combining the Bragg law and the plane-spacing equation applicable to the particular crystal involved, we can get a general relation which will predict the diffraction angle for any set of planes. For example, if the crystal is cubic, then

$$n\lambda = 2d\sin\theta$$

and $$\frac{1}{d^2} = \frac{(h^2 + k^2 + l^2)}{a^2}$$

Combining these equations, we get

$$\sin\theta^2 = \frac{\lambda^2}{4a^2}(n^2h^2 + n^2k^2 + n^2l^2)$$

This equation gives, for a particular incident wavelength λ and a particular cubic crystal of unit cell size a, all the possible Bragg angles at which diffraction can occur from the planes (hkl).

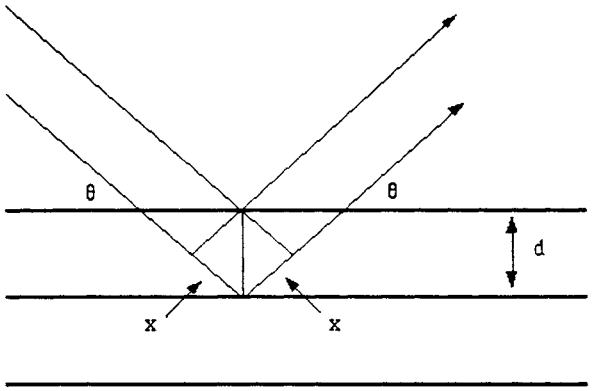

Figure 2-4 Reflection of x-rays from two planes of atoms in a solid.

However, it should be mentioned that the intensity of the diffraction lines is also affected by the following six factors. They are polarization factor, structure factor, multiplicity factor, Lorentz factor, absorption factor, and temperature factor. This results in the phenomena that not all the diffraction lines can be observed. The interested reader is referred to Ref. 28.

During measurement, the surface of the sample should be kept very flat parallel to the bottom of sample holder, which is very important to get a good signal. Fortunately the silicon substrate can be used as an indication about this alignment. Each time if a very strong silicon (400) peak appears, it means the alignment is good.

The XRD used in the present work is a PAD-II Diffractometer manufactured by Scintag. Inc. Using Cu-K_α radiation, the measurements were carried out under a voltage of 30 V and a current of 20 mA.

2.5 Film Thickness Measurement and Atomic Force Microscopy

The thickness measurement is carried out by first chemical etching to make a step then measuring the height of that step by atomic force microscopy (AFM). The chemical etching procedure is shown as follows:

First, we put a drop of HMDS adhesion promoter onto the thin film surface and let the adhesion promoter cover the whole area, and then applied a small dot of positive photo resist (AZ1512) onto the center of the surface. After that, the sample was dried in a box oven for 1 hour at 90°C. When it was dried, the sample was put into the solution of aqua regia (HNO_3: HCl: H_2O = 3: 1: 2). When the unwanted region of the film was etched out (approximately 3 min), take out the sample and by then there is left only the central region protected by the photoresist. Then use acetone to get rid of the photoresist and use ethanol to rinse the sample, and use nitrogen gas to blow the sample to make it dry. This process is shown in Fig.2-5.

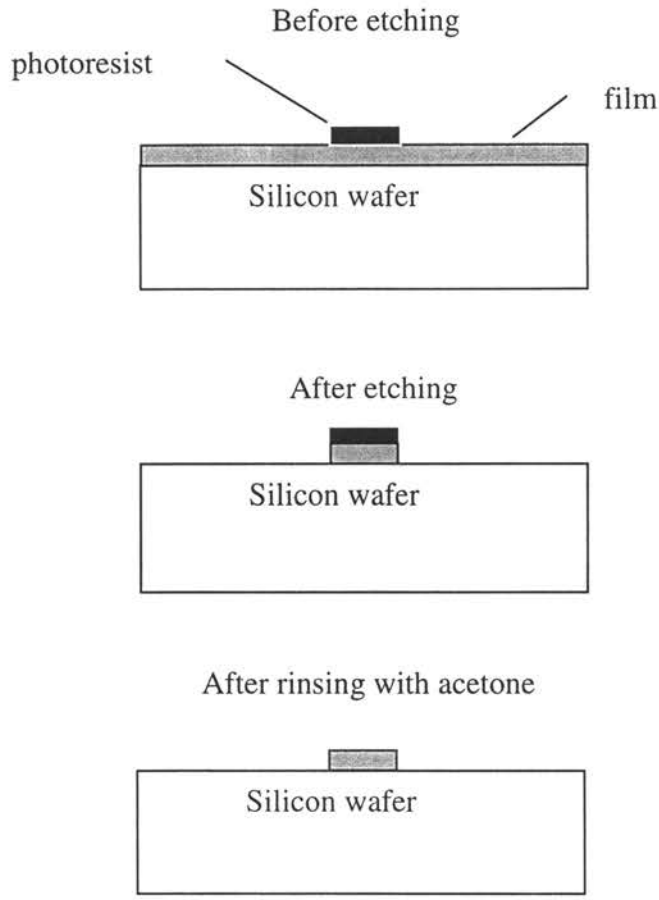

Figure 2-5 An illustration of the chemical etching process

The working principle of contact mode AFM is shown in Fig.2-6 [29]. It is operated by scanning a tip attached to the end of a cantilever across the sample surface while monitoring the change in cantilever deflection with a split photodiode detector. The tip is a kind of silicon nitride which contacts the surface through the adsorbed fluid layer on the sample surface. A feedback loop maintains a constant deflection between the cantilever and the sample by vertically moving the scanner (z) at each (x, y) data point to maintain a "setpoint" deflection. The distance that the scanner movers vertically at each (x, y) data point is stored by the computer to form the topographic image of the sample surface.

The height value of the step (i.e. thickness) is determined through the Real-Time Operation feature of the control software. In the present research, the thickness measurement is quite important because this will affect the accuracy of the magnetization measurement of the sample, because magnetization is the product of the sample's total magnetic moment divided by the sample's volume, and the volume is the product of area times thickness. During thickness measurement, usually over 8 positions around the perimeter of the sample were measured, and the final thickness value is the average of all the measurement results. The error bar is determined from the product of standard deviation divided by average value. The error bar was less than 10% for most of the samples.

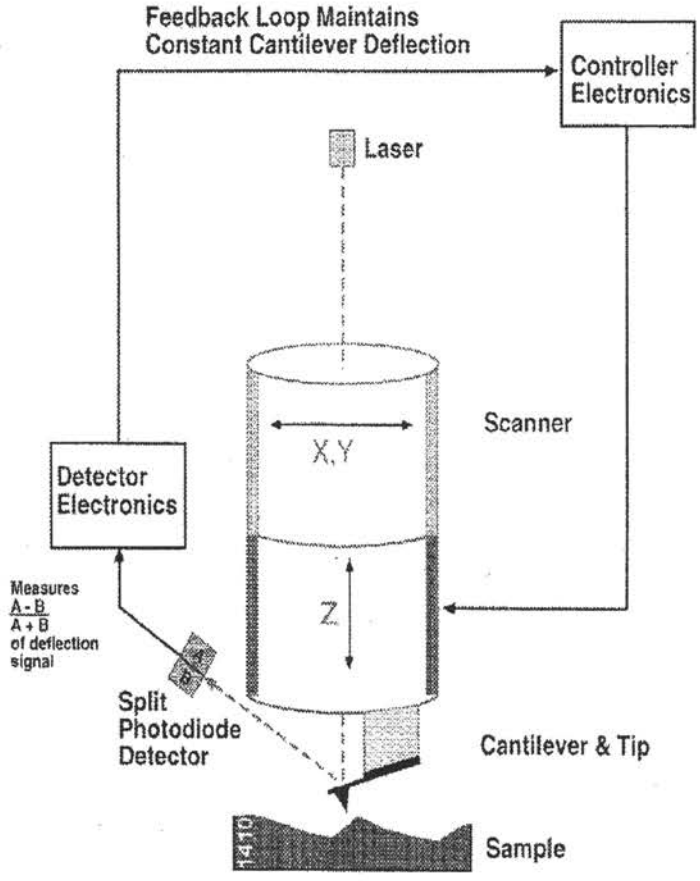

Figure 2-6 Schematic illustration of a contact mode AFM [29]

The AFM used for this study is a NanoScope™ Scanning Probe Microscope manufactured by Digital Instruments, Veeco Metrology Group, Santa Barbara, CA.

3. THE EFFECT OF THE SUBSTRATE TEMPERATURES AND NITROGEN PRESSURES

3.1 Results for Composition Measurement

The Fe-N thin film samples were deposited onto Si(100) substrates with 300 nm of thermal SiO_2 on the surface. The nitrogen pressure levels were systematically varied from 0.1mTorr to 40mTorr. One series of films was deposited at the substrate temperature of 20°C and one series at 250°C.

Film thicknesses were found to vary from 114 nm to 235 nm, depending on the nitrogen pressure. Thus the deposition rate ranged from 0.021 nm/s to 0.044 nm/s.

Figure 3-1 shows the relation between film average nitrogen content and nitrogen pressure for the series deposited at 20°C and the series deposited at 250°C. Previously reported PLD results did not contain measurements of the actual amount of N incorporated into the films [22]. For each series, film average nitrogen content increases with nitrogen pressure, with a functional dependence that is less than linear. For the 250°C series, the film average N content appears to saturate at about 11 at %. For a given N pressure, it appears that less N actually gets incorporated into the film at growth temperature of 250°C than at 20°C.

Fe-nitrides are reported to be only metastable [9, 30]. A possible explanation of why less N is incorporated at 250°C than at 20°C is that at the higher substrate temperature, more N on the growing film surface might be desorbed before it can be incorporated into the film.

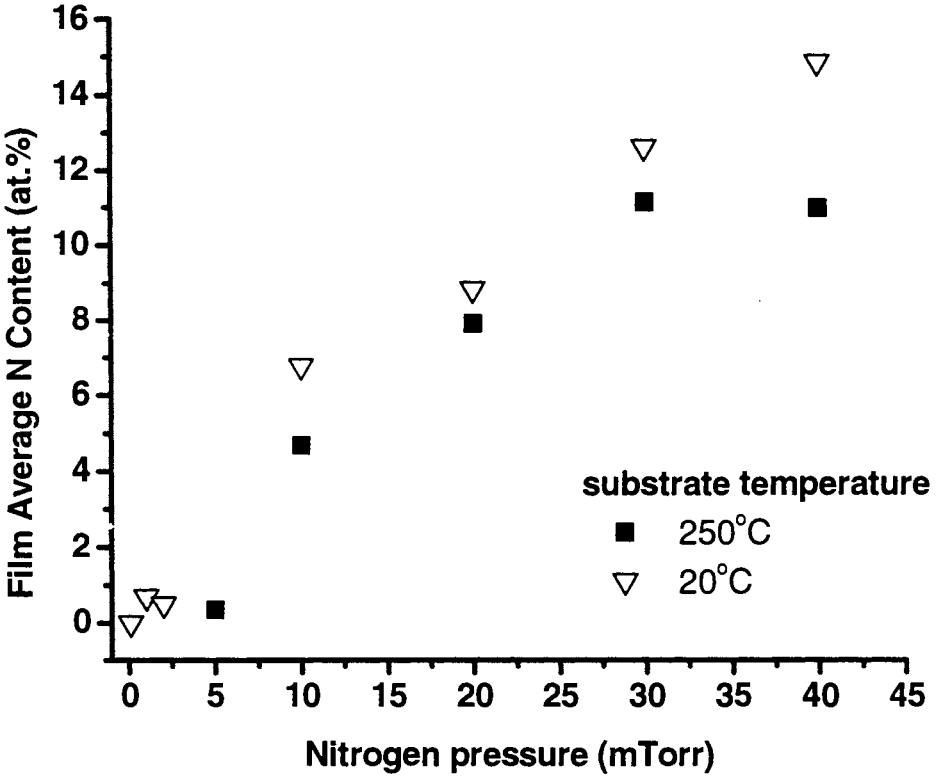

Figure 3-1 The dependence of film average nitrogen content on nitrogen pressure and substrate temperature.

3.2 Results for Magnetic Properties

Figure 3-2a shows the dependence of film magnetization on nitrogen pressure, and Fig.3-2b shows the dependence of film magnetization on film average nitrogen content. For low nitrogen pressures and nitrogen contents, the film average M_s is within experimental uncertainty of the pure Fe value. As nitrogen pressure is increased, the film average magnetization decreases, for both series of films (T_{sub} of 20°C and 250°C) in the same general manner. Out to about 7 or 8 at.% nitrogen, the film average M_s decreases only slightly. Then in the region from 8 to 11 at.% N, M_s drops rapidly, becoming less than 300

emu/cm^3, and remaining in the range of 200 to 300 emu/cm^3 out beyond 14 at.%. No magnetization increase similar to that observed by Yoshitake and Ohkoshi [22] was observed in the series deposited at 250°C.

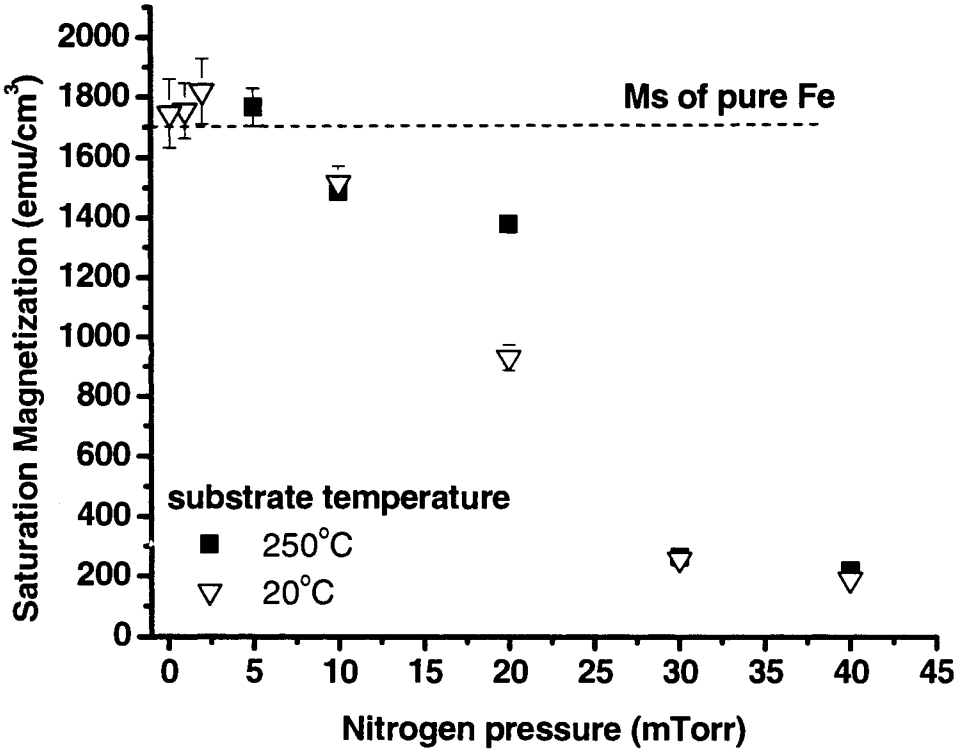

(a)

Figure 3-2(a) The dependence of film average saturation magnetization M_s on the nitrogen pressure for films deposited at 20°C and 250°C.

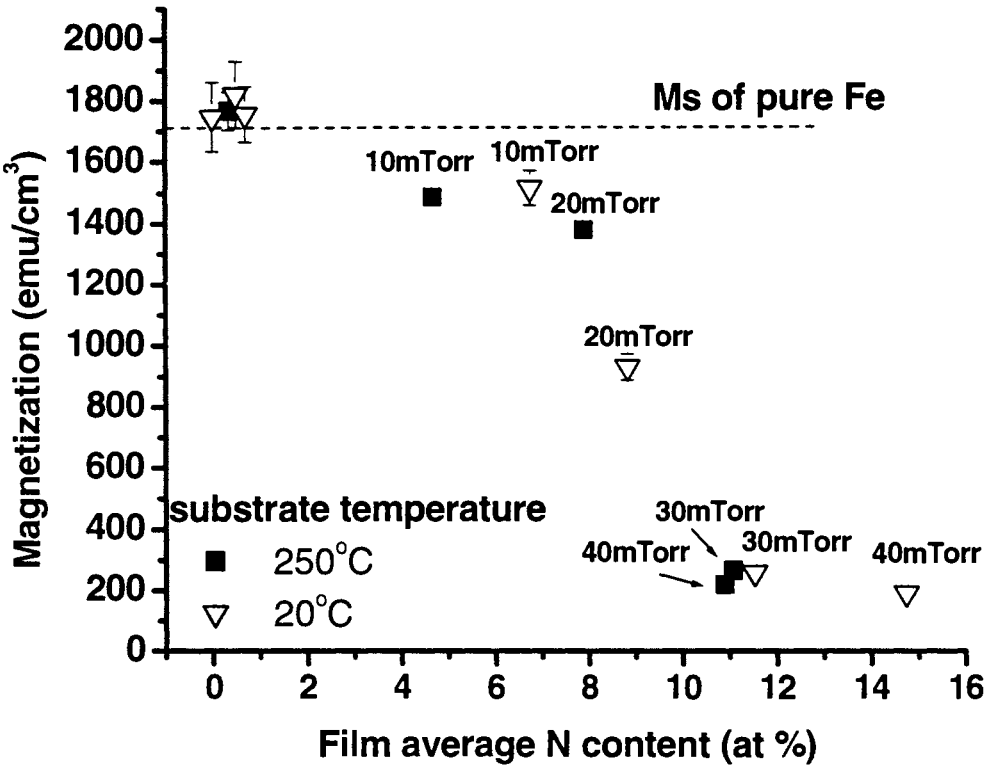

(b)

Figure 3-2(b) The dependence of film average saturation magnetization M_s on the film average nitrogen content for films deposited at 20°C and 250°C.

3.3 Results for XRD Measurement

Figure 3-3 presents the XRD results for the 20°C substrate temperature series. For low nitrogen pressure, a peak is observed at 2θ of 44.5 degrees, which can be identified as α-Fe (110). No other α-Fe peaks are observed. This is may be due to (110) texture in the film. When nitrogen pressure is increased from 0.1mTorr to 2.0mTorr, the peak at 44.5 degrees splits and one of the two peaks shifts to lower angle. This appears to correspond to a tetragonal distortion and the formation of α′-FeN martensite, which has a base centered tetragonal (bct) structure. The splitting observed for the 2mTorr sample corresponds to a difference in *d* spacing of 0.002 nm. When the ambient pressure of N is increased to 10mTorr, the tetragonal distortion becomes much more severe. The intensity of the α-Fe peak decreases greatly and α′-Fe peak moves to 43.5 degrees. α′ and α peaks are by then totally separated. In Figure 3-2, the magnetization of the 20°C sample series shows a moderate decrease when the nitrogen content reaches 7 at.%, and the structure shows this larger tetragonal distortion. It is known that the magnetic properties of Fe and Fe-rich structures are volume-sensitive with a strong connection between structure and magnetism [9]. Some groups report that M_s of α′-Fe could be larger than pure iron [31], but here it seems that the formation of the larger-distortion α′-FeN martensite results in a moderate decrease of M_s. With the increase of nitrogen pressure to 20 mTorr and 30 mTorr, a peak near 43 degrees is observed which can be identified as ε-Fe_3N(111). The magnetization of these samples decreases steeply in Fig. 3-2 with the formation of ε-Fe_3N phase. No XRD peaks were observed for the sample deposited at 40mTorr. It appears to be amorphous or might have very fine nano-grains.

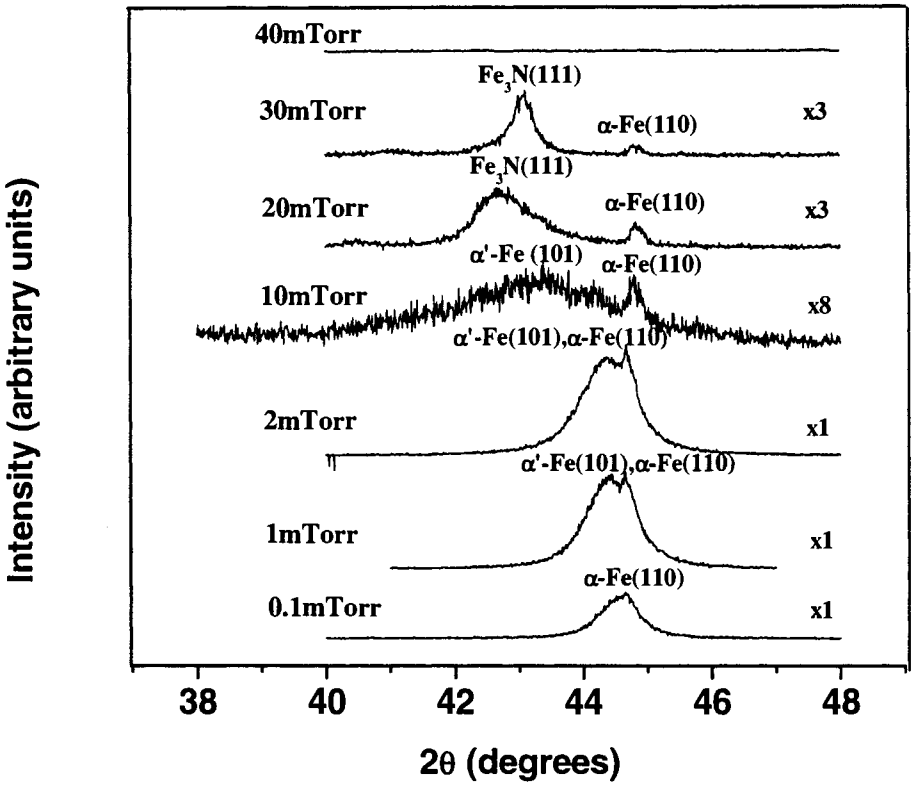

Figure 3-3 The XRD results for the 20°C substrate temperature sample series.

Figure 3-4 provides XRD data analysis for the 250°C sample series. When the nitrogen pressure is 5mTorr, there is very little nitrogen incorporated into the film (shown in Fig.1) and thus only the α-Fe (110) peak appears, near 44.5 degrees. When the nitrogen pressure is increased to 10 mTorr, in addition to the α-Fe (110) peak, a peak is observed around 43.5 degrees, which can be identified as α′-Fe (101) with the bct structure. Peaks are also observed at 41.5 and 47.5 degrees which can be identified as another nitride phase called γ′-Fe_4N. Due to the formation of iron nitride, the magnetization of the sample deposited at 10 mTorr began to decrease in Fig.3-2. Although possessing a higher atomic percent of nitrogen, the sample deposited at 20 mTorr has the same phases present as the sample deposited at 10 mTorr sample, but with different relative amounts, and different crystallographic texture. The γ′-Fe_4N (111) peak has a lower intensity in the 20 mTorr film than in 10 mTorr film. This may be due to (200) texture in the sample deposited in 20 mTorr. The magnetization of the 20 mTorr sample shows a small decrease compared to the 10 mTorr film (Fig. 3-2). When the nitrogen pressure is increased to 30 and 40 mTorr, the γ′-Fe_4N peaks disappear and a peak is observed around 43 degrees, which can be identified as the ε-Fe_3N (111) peak. Just as in the series deposited at 20°C, the magnetization decreases steeply with the formation of ε-Fe_3N phase. This agrees with theoretical predictions that Fe_3N should have lower magnetization than Fe_4N or α-Fe [9]. In the sample deposited at 40 mTorr, there is also a peak around 36.3 degrees which might be identified as iron oxide, although the oxygen content measured by XPS is near 2 at.%.

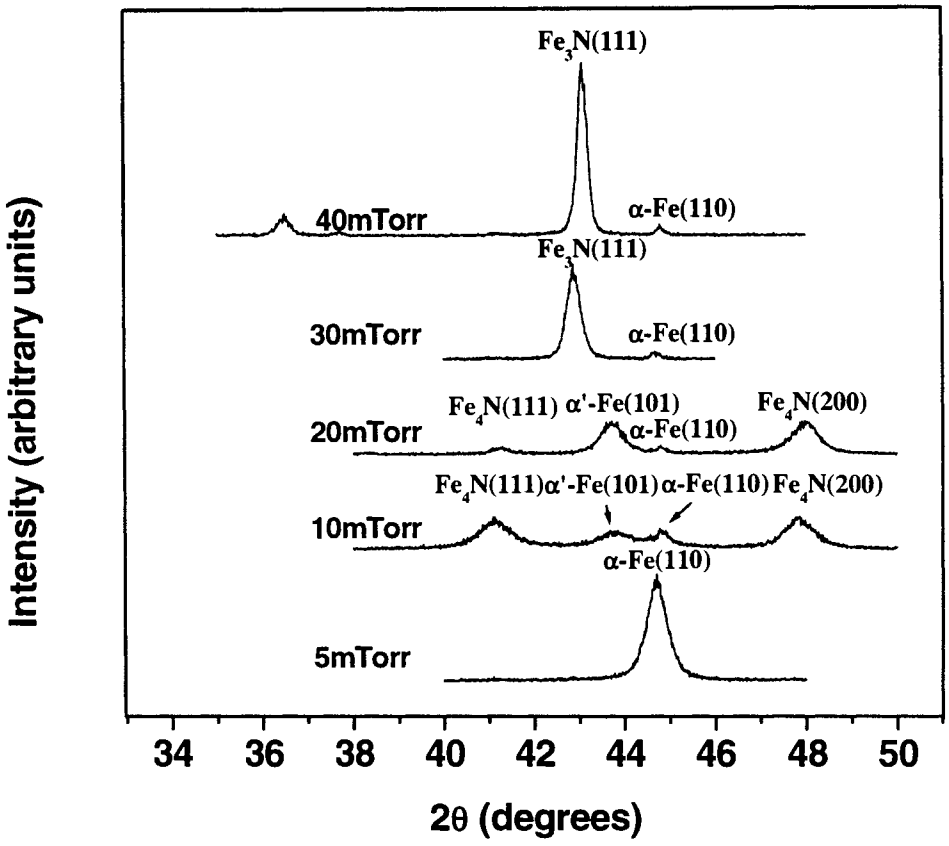

Figure 3-4 XRD results for the 250°C substrate temperature sample series.

3.4 Discussion

In the 20°C series, for low nitrogen pressures (0.1, 1, and 2 mTorr), α-Fe and α′-FeN martensite with a small tetragonal distortion are formed. For 10 mTorr nitrogen, the same two phases form, however the α′-FeN martensite shows a much larger apparent tetragonal distortion. For the nitrogen pressures above 10 mTorr, the next phase that forms is ε-Fe_3N (shown in Fig.3-3). In the 250°C series, for low nitrogen pressure (5 mTorr) a more distinct α-Fe (110) peak is observed, and for increasing nitrogen (10 and 20 mTorr) the next phase formed is γ′-Fe_4N. For higher nitrogen pressures yet (30 and 40 mTorr), ε-Fe_3N is formed which shows sharp and narrow peaks. From the XPS results, for both the 20°C series and the 250°C series, at low nitrogen pressure (less than 10mTorr) the actual nitrogen atomic percent is very small (1<at.%), and for even the highest nitrogen pressures used in this investigation the actual average nitrogen content is less than 15 at.% (show in Fig.3-2b). For these compositions and temperatures, the bulk phase diagram predicts α-Fe phase for very low nitrogen content and mixture of α-Fe and γ′-Fe_4N rather than ε-Fe_3N for the higher nitrogen contents (up to about 20 at.% nitrogen) [7]. Therefore the behavior of the 250°C series is closer to the equilibrium process or what we expect on the basis of the bulk phase diagram than the behavior of the 20°C series. This can be understood by considering the following model: Atoms on the growing film surface are free to diffuse much more easily than atoms in bulk at the same temperature. How easily they diffuse on the surface (i.e. how much they move per unit time) is determined by substrate temperature. Those atoms on the surface can move until they are constrained by subsequently-deposited atoms. How much time they have to move is determined by deposition rate. Thus for the same deposition rate but higher

substrate temperature, atoms on the surface have more opportunity to find energy minima. The structure produced will be closer to bulk or equilibrium structure. Indeed, it is sometimes true in thin films that at low substrate temperature, the phase that forms first is a higher temperature phase or non-equilibrium phase rather than the bulk equilibrium phase for that temperature, due to kinetic constraints.

Figure 3-2b shows that the two series of films show the same general dependence of film average saturation magnetization on film average nitrogen content. The magnetizations of the films decrease as the overall film average N composition increases. However, some specific features show that it is not just average N content that is important, but specifically what phases are present, and their relative amounts and their magnetic moments. The total magnetization of a given sample should be equal to the sum of the magnetizations of the different phases present, weighted by their relative amounts in the sample.

The films with less than 1 at.% nitrogen appear to consist of predominantly α-Fe phase or a mixture of α with an α′ that shows a very small tetragonal distortion. These films show M_s values quite close to pure α-Fe, as one might expect. For nitrogen contents up to about 8 at.%, the films show a moderate decrease of M_s compared to the pure-Fe value. In the case of the film deposited at 20°C and 10 mTorr N, it appears to consist of a mixture of α phase with a large amount of α′-FeN martensite phase with a large tetragonal distortion. In the case of the films deposited at 250°C, and 10 and 20 mTorr, they appear to consist of a mixture of α and α′ phase with a large tetragonal distortion, and γ′-Fe_4N. In the region beyond 8 at.% nitrogen, film average magnetization decreases rapidly. These films from both series appear to consist of mixtures of ε-Fe_3N + α, with the amount of α decreasing for

increasing nitrogen pressure. Thus it appears that for the films of this study, the magnetizations of both the α' phase with the large tetragonal distortion and the γ'-Fe_4N phase are moderately less than that of pure Fe, and relatively similar to each other. The ε-Fe_3N phase would appear to have much lower magnetization than either of these others. These results are supported by theoretical predictions that $M_{s,\alpha\text{-}Fe}>M_{s,Fe4N}>M_{s,Fe3N}$ [9]. The experimental values for the magnetization of α-Fe, γ'-Fe_4N, and ε-Fe_3N have been reported as 220 $JT^{-1}kg^{-1}$, 178 $JT^{-1}kg^{-1}$, and 123 $JT^{-1}kg^{-1}$ respectively [32], which also support the present results.

For the sample deposited at 40 mTorr and 20°C, we did not observe any peaks attributed to the Fe-N film with XRD. This could indicate an amorphous film although it might have nanograins of size and/or volume fraction below the detection limit of XRD. This sample has the highest nitrogen content of any of the films (14.7 at.% N). In general, when metals or simple compounds are deposited at room temperature or above, they tend to form crystalline thin films, rather than amorphous ones. However, there are other known Fe-metalloid systems (e.g. the Fe-B system, and ternary and quaternary alloys based on it) in which one can produce amorphous material by rapid quenching or thin film deposition methods. There have been a few reports in the literature, of amorphous Fe-N powder or bulk material having been fabricated by ball-milling [32,33] and ion-implantation [34,35], and amorphous Fe-N thin films by ion beam deposition [36] and facing targets sputtering [37]. Another possibility is that the film has a very fine nanocrystalline structure which can not be detected by XRD θ-2θ scans. In order to further investigate this, TEM-based structural investigations would be needed.

In the present work, we have replicated the nitrogen pressures and substrate temperatures of Yoshitake and Ohkoshi's previous PLD work [22], but did not see enhanced saturation magnetization values in the same region of temperature and nitrogen pressure that they did. They reported an M_s of 2300 emu/cm^3 for the film deposited at 250°C with 30 mTorr nitrogen pressure. Under these conditions we did observe the composition that would correspond to $Fe_{16}N_2$, i.e. ~11 at.% N (Yoshitake and Ohkoshi did not report composition measurements that we can compare to). However, we saw mainly ε-Fe_3N phase (so called, although reported to have a composition range of ~15 to ~33 at.% N [31]), plus a little α-Fe. In Yoshitake and Ohkoshi's work, they reported instead a structure identified as α* bct Fe-N (a new phase which they propose, with a bct structure and lattice constants a = 0.285nm and c = 0.287nm). The difference between their work and the present work might be attributed to the different deposition rates. In their study, a deposition rate of 0.25 nm/s was reported while in the present work the rate is 0.021 nm/s to 0.044 nm/s. The former is thus 6 to 12 times higher. For higher deposition rates, atoms have much less time to find low energy positions before being constrained by other deposited atoms. This could thus produce a different structure that is much more highly non-equilibrium. Our process gives a phase mixture (ε-Fe_3N + α) which is also non-equilibrium, but would appear to be closer to equilibrium than Yoshitake and Ohkoshi's process. Actually, in order to get α″-$Fe_{16}N_2$ phase, a non-equilibrium deposition process is required. At equilibrium, the phase transformation in the bulk Fe-N systems upon cooling is: γ-Fe:N (fcc)→α-Fe (bcc)+ γ′-Fe_4N (fcc). With rapidly quenched bulk material, there is: γ-Fe:N (fcc)→α′-Fe:N (bct), and upon annealing: α′-Fe:N (bct)→α″-$Fe_{16}N_2$ (bct) [8]. It is interesting to note that Yoshitake and Ohkoshi did not

propose that the increased moment in their samples is due to α''-$Fe_{16}N_2$ phase (which they did not observe), but rather, speculate that it is due to a heterogeneous state of γ'-Fe_4N precursors within their proposed α^*-phase.

4. THE EFFECT OF ANNEALING

4.1 VSM and MFM Measurement Results before Annealing

The hysteresis loops determined by VSM for the samples deposited at 20°C are shown in Fig.4-1.

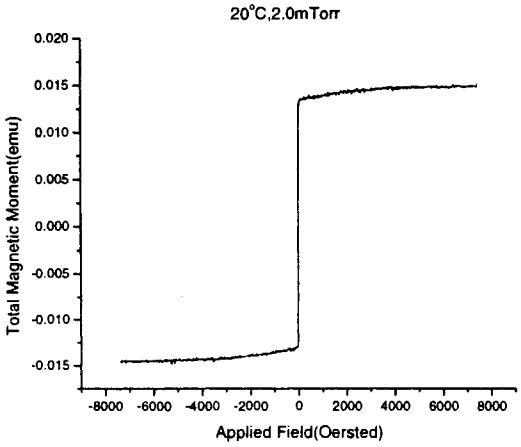

(a)

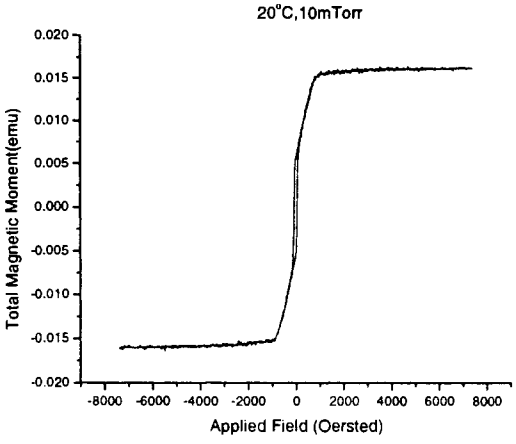

(b)

Figure 4-1 Hysteresis loops of the samples deposited at 20°C temperature: a) 2mTorr; b) 10mTorr.

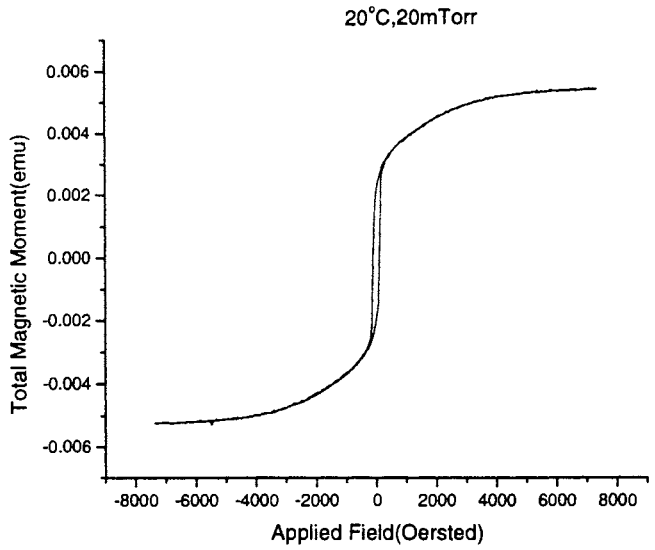

(c)

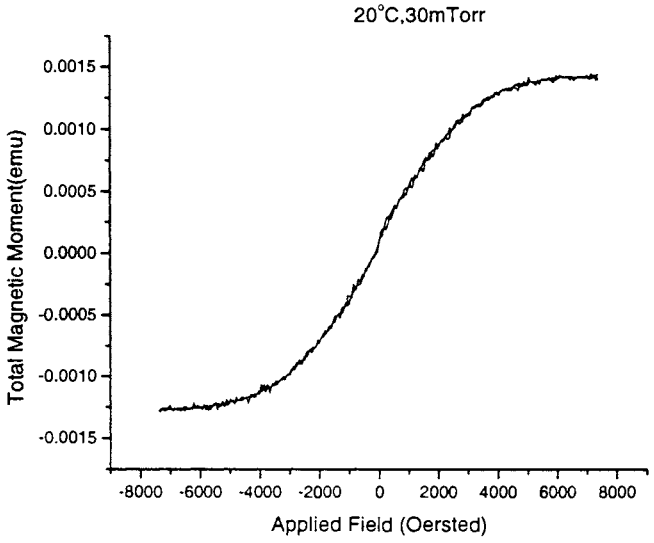

(d)

Figure 4-1 Hysteresis loops of the samples deposited at 20°C temperature: c) 20mTorr; d) 30mTorr.

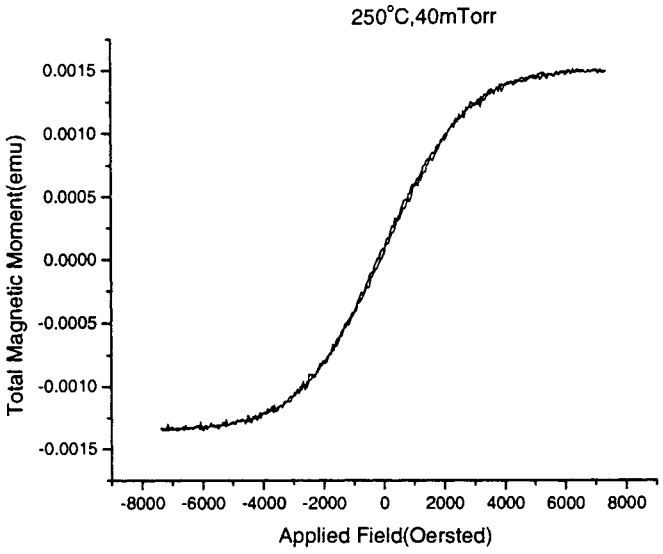

(e)

Figure 4-1 Hysteresis loops of the samples deposited at 20°C temperature: e) 40mTorr.

For each sample, its hysteresis loops were measured along two different orthogonal directions in the plane and it was found that these two hysteresis loops are very close.

The shapes of the hysteresis loops vary significantly corresponding to the nitrogen pressures (or nitrogen contents). With the increase of the nitrogen content, the samples become harder and harder to saturate. During the VSM measurement, the external magnetic field was applied parallel to the sample's surface. One possible explanation is that the preferable directions of the magnetizations could be changing from in-plane direction to the direction normal to the plane. However, there are two other possible explanations for this phenomenon which should be considered. One is that the magnetization is still in-plane, and the external magnetic field is being applied along the hard axis. This explanation should be excluded because the hysteresis loops measured along two orthogonal directions of the

sample's surface do not show any difference. The other is that for the samples deposited at high nitrogen pressure, there may form local anisotropic magnetization and it is still in-plane, which will also make the sample hard to saturate. However, if so, there should be a large coercivity and this does not appear in the hysteresis loops. Therefore the second explanation can be excluded too. Shown in Fig. 4-1, for the samples deposited at 2mTorr, in-plane magnetization component dominates. For the samples deposited at 10mTorr and 20mTorr, the magnetization could have an increasing perpendicular component. For the samples deposited at 30mTorr and 40mTorr nitrogen pressures, the film could have a preferable magnetization normal to the substrate plane. It is known that stress can have a strong effect on the magnetic properties of the thin films. Through magnetoelastic coupling, isotropic in-plane compressive stress can cause a perpendicular magnetic anisotropy component for materials with positive magnetostriction, and the larger the stress, the larger the perpendicular magnetic anisotropy. Film stress determined from the samples deposited at 2mTorr, 20°C and 20mTorr, 20°C is shown in Fig. 4-2. The negative curvature means that they both exhibit an in-plane compressive stress, and the curvature determined from the 20mTorr sample (-2.0294×10^{-7} at the maximum of the curve) is larger than that from the 2mTorr sample (-1.2968×10^{-7} at the maximum of the curve), which means that the 20mTorr sample possesses a larger compressive stress. It is reasonable since more introduced nitrogen interstitial atoms will introduce more stress. The equation for the curvature is:

$$K=\frac{\left|\frac{d^2y}{dx^2}\right|}{\left[1+\left(\frac{dy}{dx}\right)^2\right]^{3/2}}$$ and the maximum, dy/dx=0. So, $K|_{max}=\left|\frac{d^2y}{dx^2}\right|_{max}$

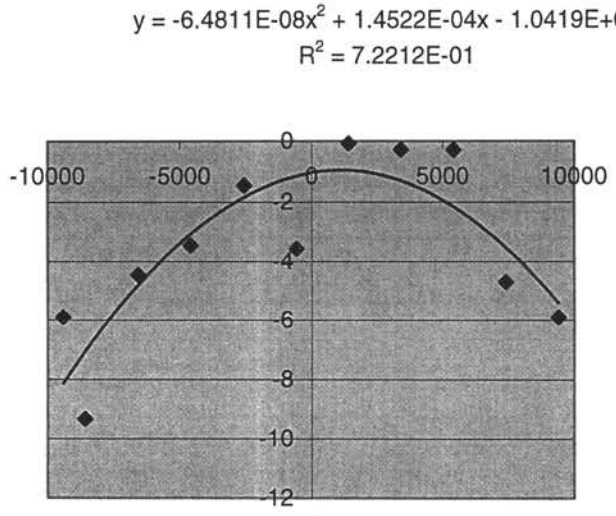

(a)

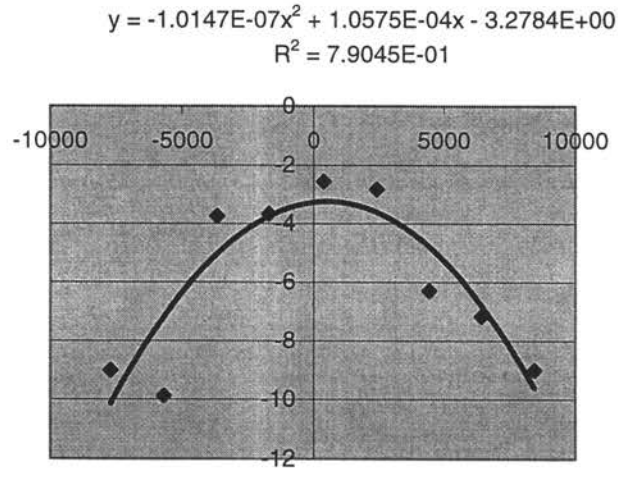

(b)

Figure 4-2 Stress measurement results for the samples (a) 2mTorr, 20°C and (b) 20mTorr, 20°C.

The MFM images for the 20°C samples series are shown in Fig.4-3. For the sample deposited at 2mTorr, XPS and XRD results (Fig. 3-1, 3-3) shows it is almost pure iron. Hysteresis loop shows an in-plane magnetization for this sample. Since the MFM is more sensitive to the perpendicular magnetization component than the in-plane component, the MFM image taken from this sample gives very weak domain configurations.

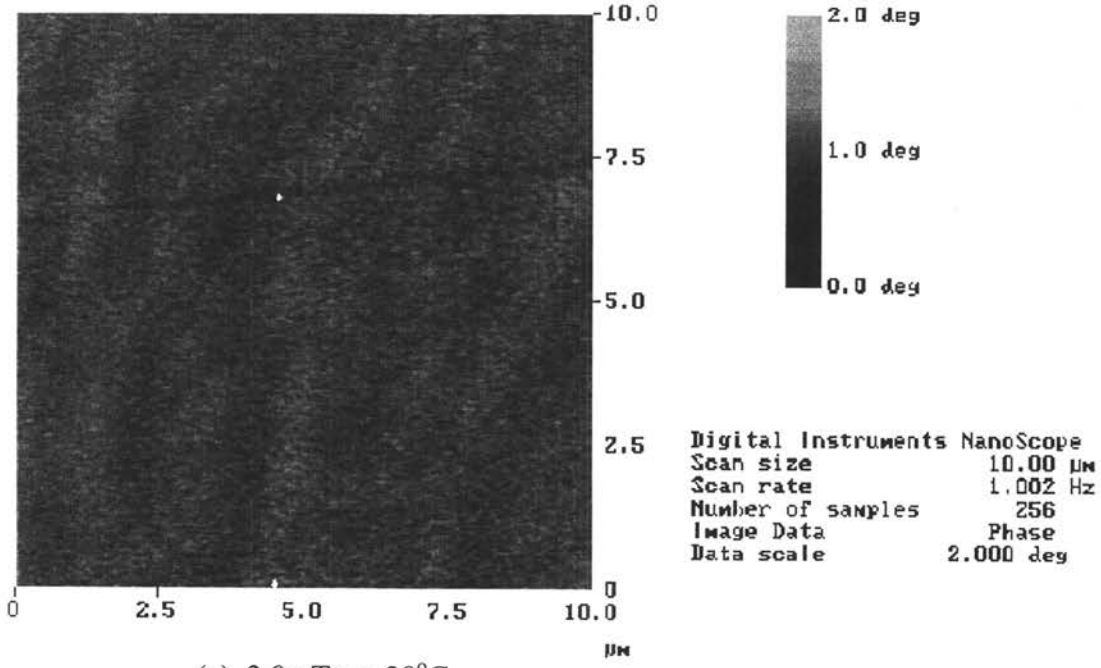

(a) 2.0mTorr, 20°C

Figure 4-3 The MFM images for the sample series deposited at 20°C.

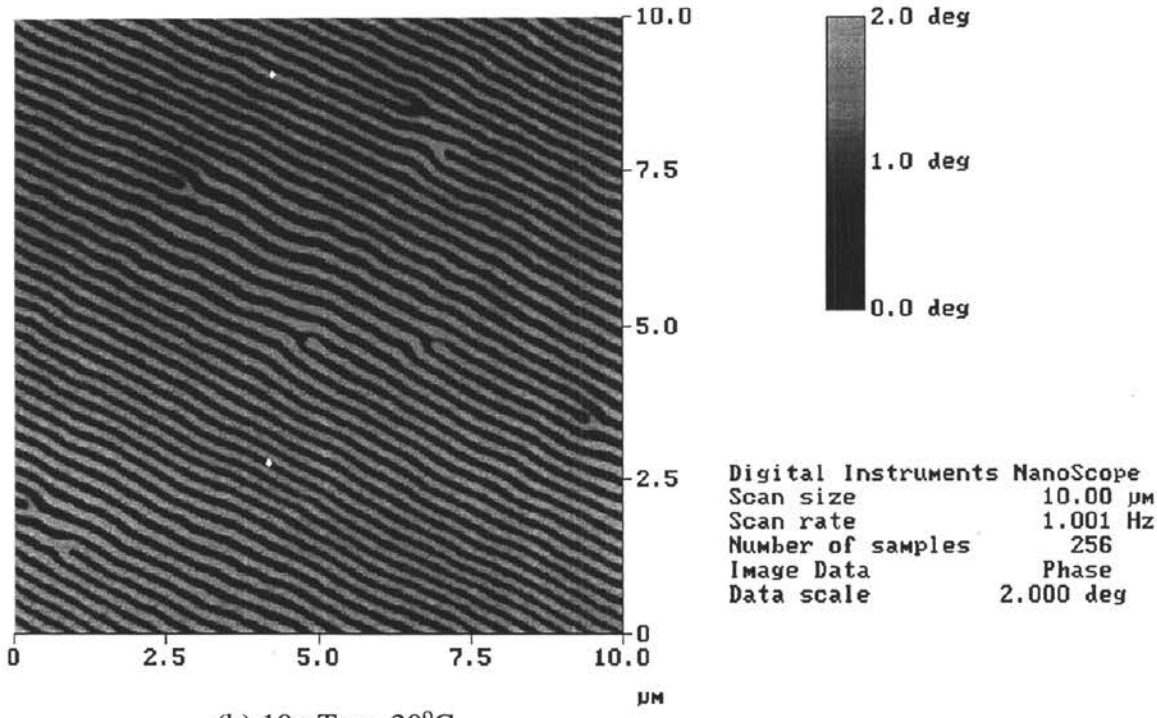

(b) 10mTorr, 20°C

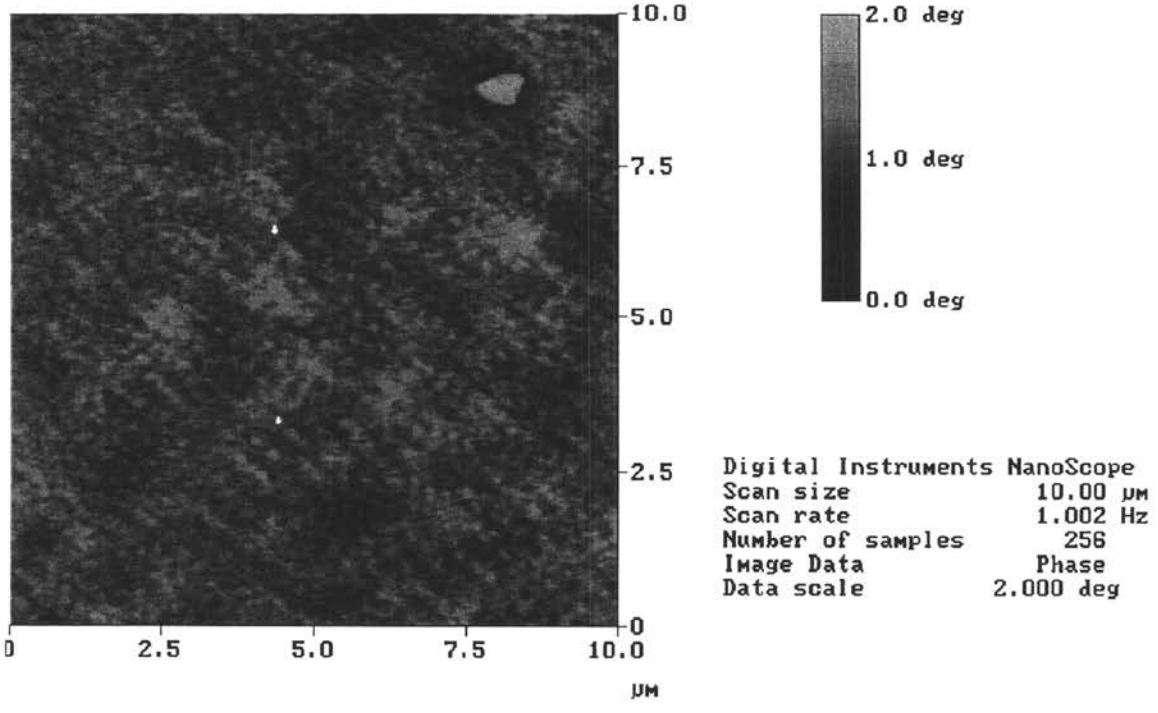

(c) 20mTorr, 20°C

Figure 4-3 (continued).

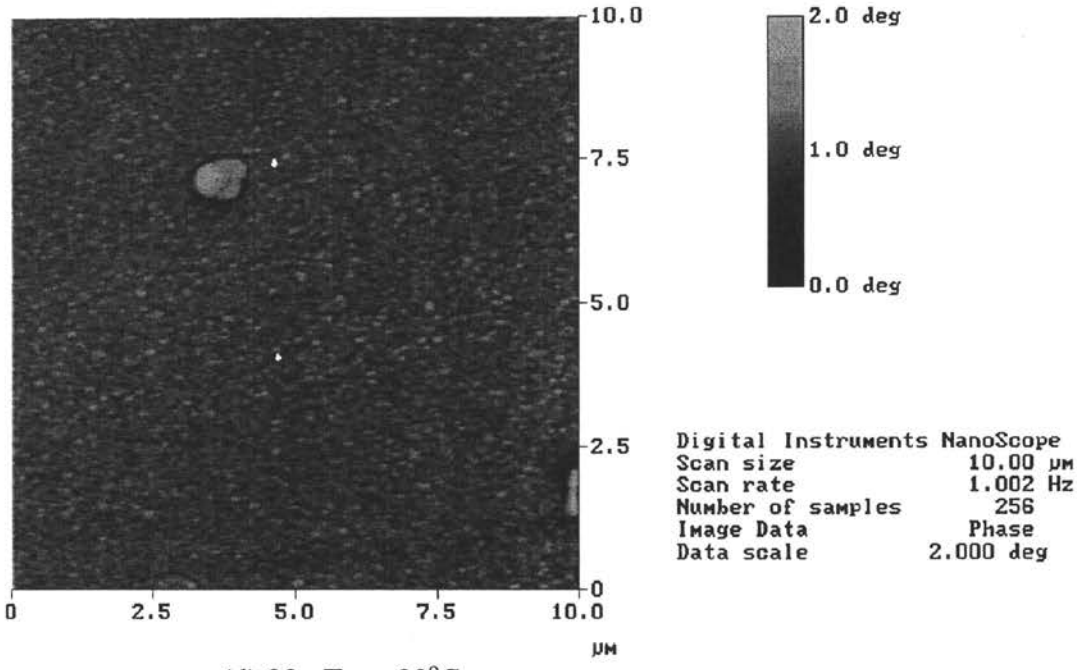

(d) 30mTorr, 20°C

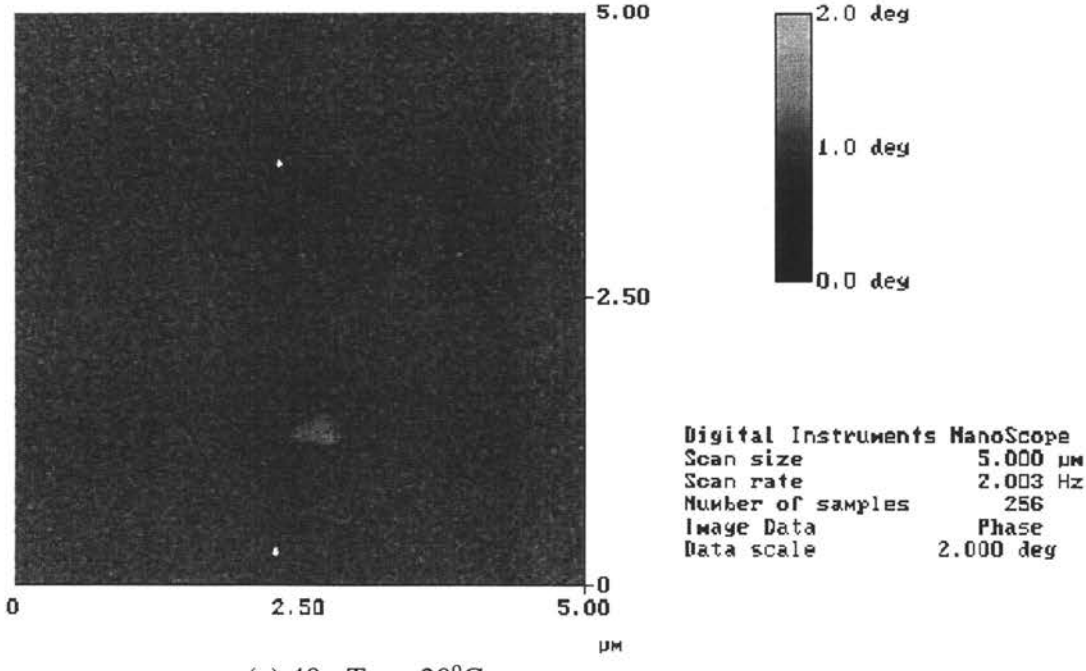

(e) 40mTorr, 20°C

Figure 4-3 (continued).

For the sample deposited at 10mTorr, stripe domains with strong contrast and preferable orientation appear. This kind of stripe domain with preferred orientation in-plane but substantial out-of-plane tipping was first proposed by Saito et al. who observed it in Ni-Fe films using the Bitter method [38]. C. C. H. Lo et al. [39,40] in their work for FeSiAl films found that the stripe domains were closely related to the perpendicular anisotropy. With the increase of the perpendicular anisotropy component, the stripe domains became coarsened and more regular. The appearance of the stripe domains demonstrate the existence of the preferable perpendicular anisotropy in the sample deposited at 10mTorr, 20°C.

It was assumed that for the sample deposited at 20mTorr there should also be stripe domains with more coarsened and regular structure since it appears to show a more preferable perpendicular anisotropy in the hysteresis loop. However, the MFM does not show such an image. Shown in Fig. 4-3c, there appear domains with much less contrast and discontinuous configuration. Irregular and discontinuous domain configuration obtained from the 20mTorr sample seems to suggest that the magnetic coupling between the domains is not as strong as that in the sample deposited at 10mTorr. The MFM images were taken from the as-deposited condition and thus there is no magnetic history effect. Consistent results were obtained when rescanning these samples using another tip, which means the effect of the tip is also excluded. One possible explanation for the lack of distinct stripe domains in the 20mTorr sample compared to the 10mTorr sample has to do with microstructure. We know that microstructure plays a very important role in determining the sample's magnetic properties. For example, if the grain size is close or larger than the domain size, the local anisotropy of the gains cannot be excluded and this could cause an irregular and discontinuous domain structure. If there are grain boundary phases they will damage the

exchange-coupling between the magnetization of the grains and this will also result in an irregular and discontinuous domain configuration Therefore, further work on the microstructure of the samples should be carried out.

Similarly, it was supposed that for the samples deposited at 30mTorr and 40mTorr, stripe domains with more regular and coarsened configuration than that of the samples deposited at 10 and 20mTorr will appear since the 30mTorr and 40mTorr appear to exhibit a more preferable perpendicular anisotropy based on the in-plane hysteresis loops. However, we did not observe any domains (see Fig. 4-3d and e). There are several possibilities. First, this may be due to the reason that the signal from these two samples are very small, smaller than the sensitivity of the MFM system. Second, the films may have a high perpendicular coercivity and remanence, so that in the remnant state they are essentially saturated, therefore no contrast appears. Third, the films may have a very low coercivity, and the tip-sample interaction might interfere with the image and we cannot see the domain walls. The last, maybe the films are superparamagnetic, and they have essentially zero remanence in any direction, and thus show no contrast. In order to check the last three ideas, a hysteresis loop obtained from a perpendicular external magnetic field is required in the future study.

From Figure 3-2, 3-3, and 4-1, we can observe the relations of the samples' magnetic properties and their compositions and phase structures. When nitrogen content is less than 1 at. % (2mTorr sample), XRD result shows a split peak, and appears to be a mixture of α-Fe and α'-Fe, with the α'-Fe peak split from the original α-Fe peak, thus representing a tetragonal distortion. Since the composition of the 2mTorr sample is close that of the pure iron film, correspondingly, the hysteresis loop of the 2mTorr sample behaves like the pure iron film and exhibits an in-plane magnetization. It should be mentioned that although the

XRD results suggest a significant α'-Fe amount is formed, the XPS results show that N content is less than 1 at. %. The average magnetization of the 2mTorr sample is also very close to that of pure iron. When nitrogen content increases to near 6.5 at.% (10mTorr), the XRD result shows that the α'-Fe peak splits a little further away from the α-Fe peak and thus forms a larger tetragonal distortion. The hysteresis loop obtained from the 10mTorr sample (Fig. 4-1b) appears to exhibit a perpendicular magnetization component, even though the phases present are still α-Fe and α' as before. This is probably due to the reason that more stress/distortion is introduced by the increased amount of interstitial N atoms. When nitrogen content keeps increasing, i.e. for the samples deposited at 20mTorr and 30mTorr, XRD shows that a new phase Fe_3N forms. It was assumed by then that the samples had even more stress and that the hysteresis loops represented even stronger perpendicular anisotropy. However, the MFM did not show any tripe domains, so the interpretation of these samples is not yet entirely clear.

The hysteresis loops for the samples deposited at 250°C temperature are shown in Fig. 4-4.

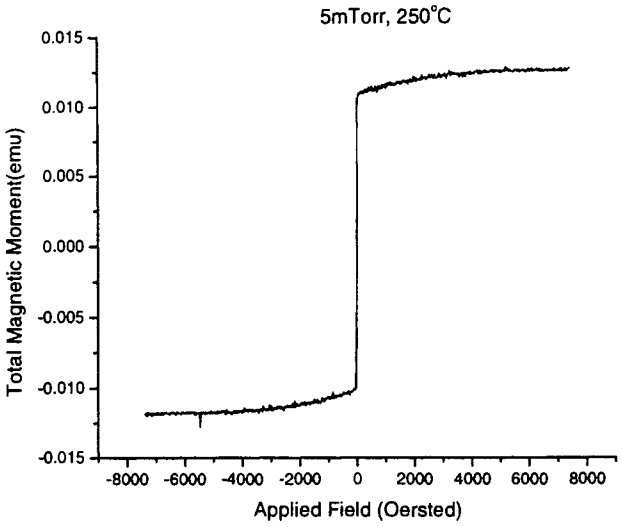

(a)

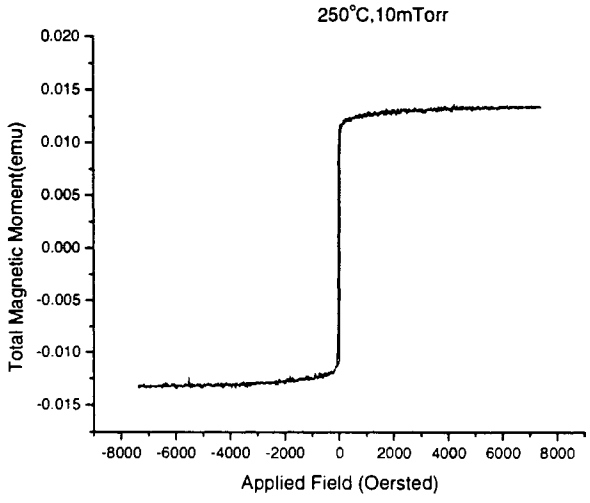

(b)

Figure 4-4 Hysteresis loops for the sample series deposited at 250°C: a) 5mTorr; b)10mTorr.

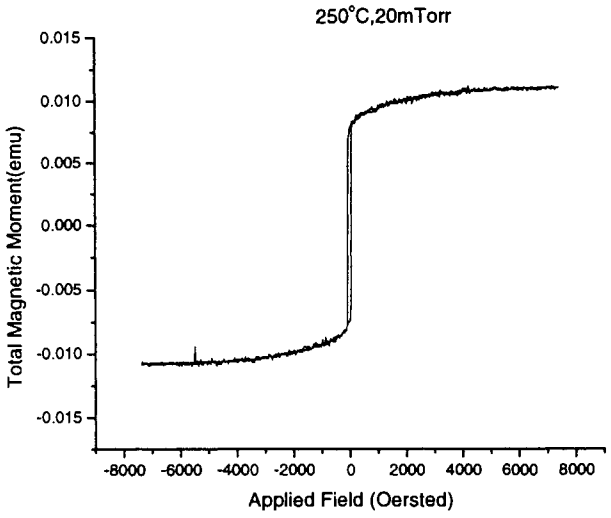

(c)

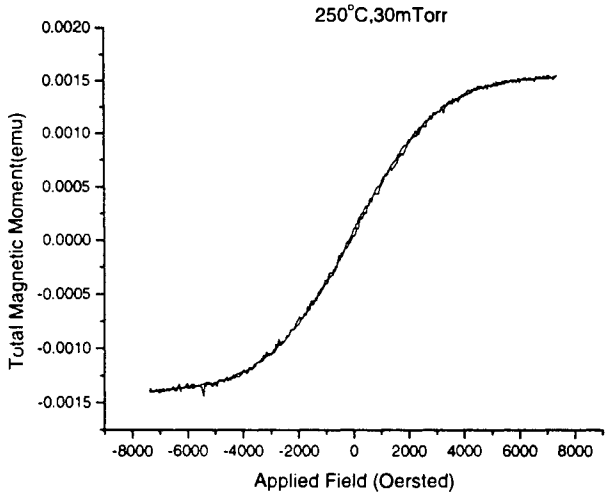

(d)

Figure 4-4 Hysteresis loops for the sample series deposited at 250°C: c) 20mTorr; d)30mTorr.

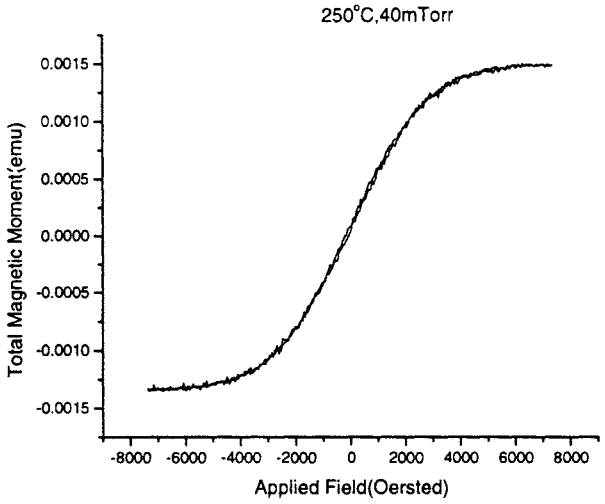

(e)

Figure 4-4 Hysteresis loops for the sample series deposited at 250°C: e) 40mTorr.

The hysteresis loops for the sample series deposited at 250°C shows a similar behavior as those in Fig.4-1 except the big difference between the loop determined from the sample deposited at 10mTorr, 20°C and that from the sample deposited at 10mTorr, 250°C. With less nitrogen content, the hysteresis loop of sample deposited at 10mTorr, 250°C behaves more like a pure iron film than does the sample deposited at 10mTorr, 20°C. It is thought that perpendicular magnetization component is exhibited more preferably in the latter because it is much harder to saturate it in the plane. This is probably due to the reason that the sample deposited at 20°C was more stressed than that deposited at 250°C. Shown in the XPS results, the 20°C sample series had higher nitrogen contents than the 250°C sample series, especially for the sample deposited at 10mTorr, which is assumed to introduce more intrinsic stress. The XRD (Fig.3-3, 3-4) results show that the sample deposited at 10mTorr,

20°C exhibits a greater tetragonal distortion than the sample deposited at 10mTorr, 250°C. Another contribution to the stress is related to the substrate temperature. A higher substrate temperature will enhance the mobility of the atoms and thus help the thin film grow more homogeneous and decrease the intrinsic stress. However, the effect of the microstructure on the magnetic properties of these samples may also be an important factor. Further study on the microstructures of these samples might be valuable.

Fig.4-5 shows the domain information of the 250°C sample series. It also exhibits a similar behavior like that obtained from the 20°C sample series except for the sample deposited at 10mTorr. For the sample deposited at 5mTorr, 250°C, its MFM image is very close to that of the sample deposited at 5mTorr, 20°C. This is reasonable since both of them obtain an in-plane magnetization and have a composition close to pure iron.

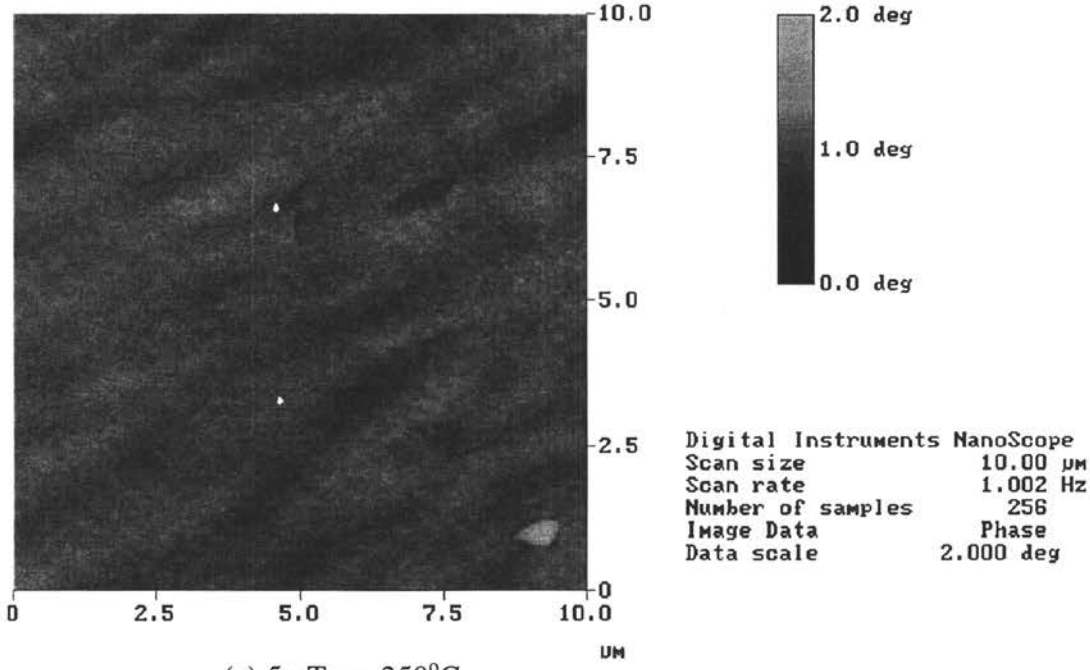

(a) 5mTorr, 250°C

Figure 4-5 The MFM images for the sample series deposited at 250°C

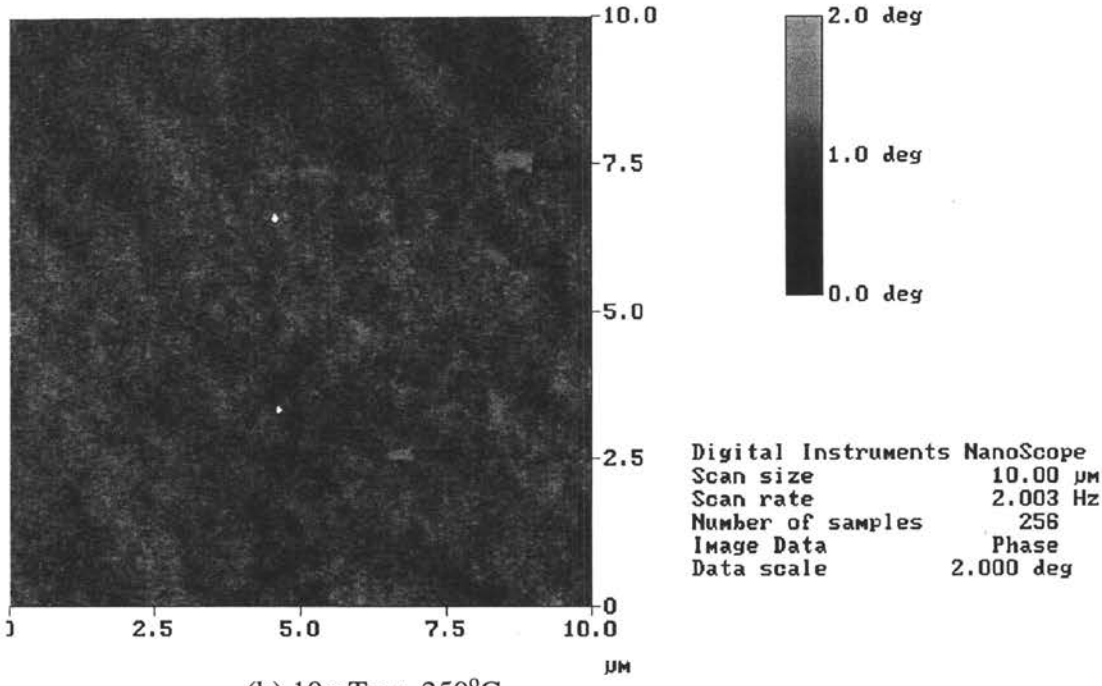

(b) 10mTorr, 250°C

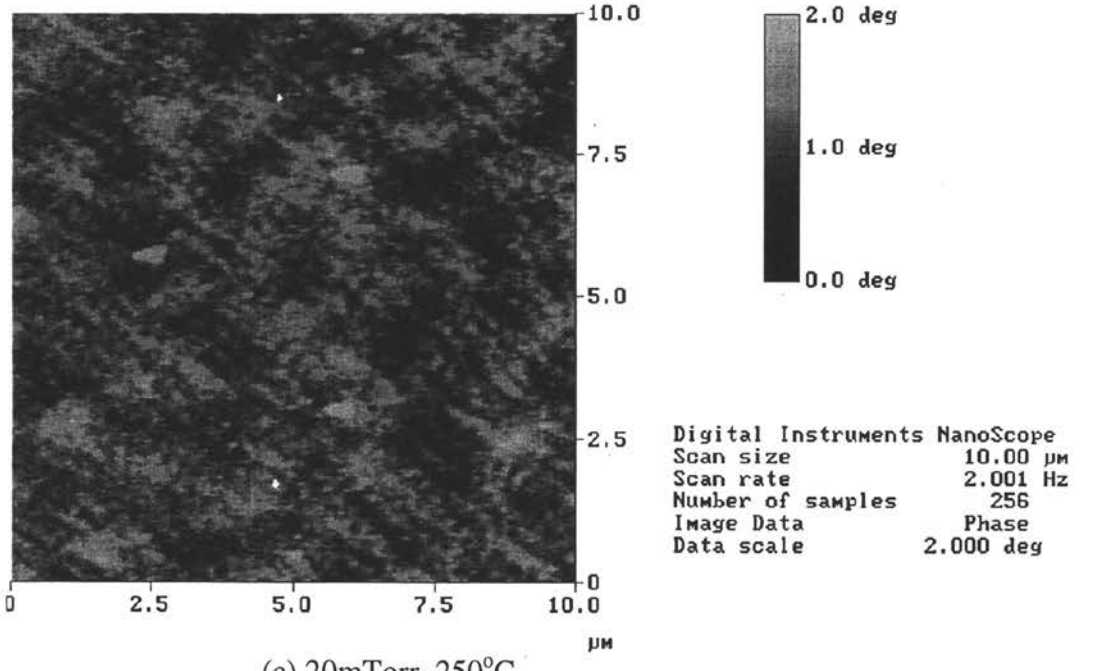

(c) 20mTorr, 250°C

Figure 4-5 (continued)

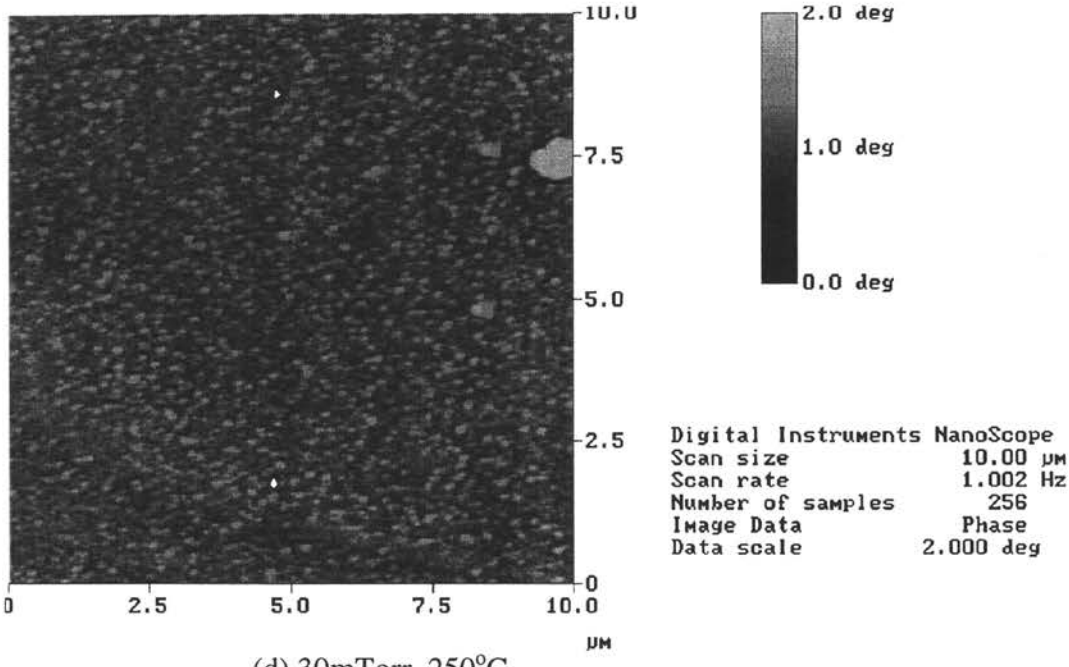

(d) 30mTorr, 250°C

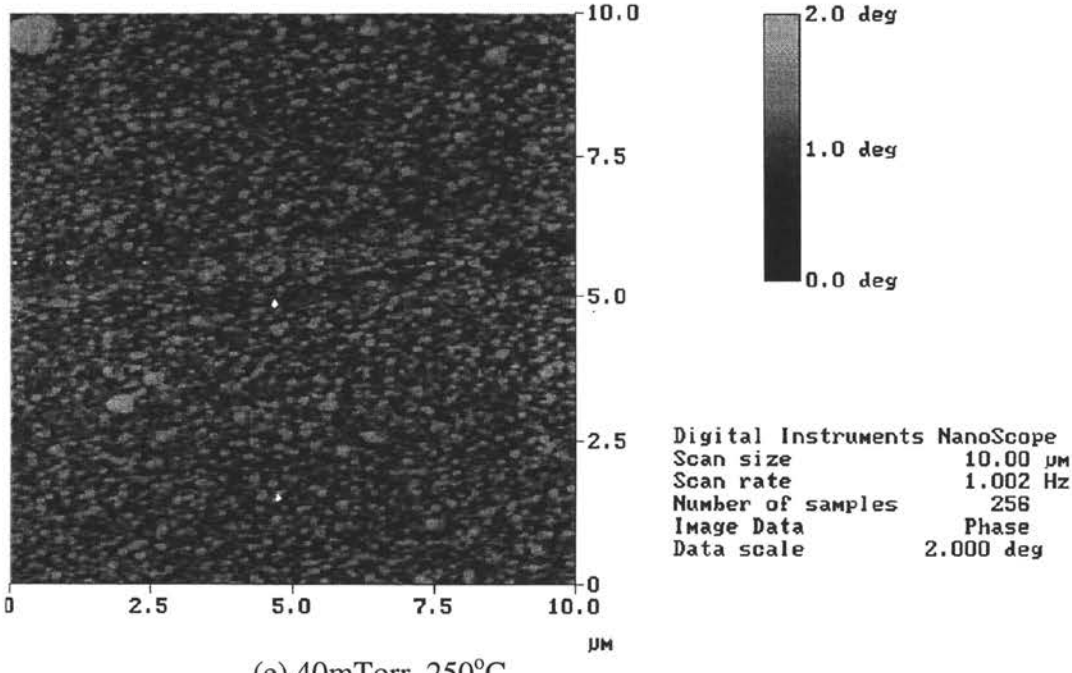

(e) 40mTorr, 250°C

Figure 4-5 (continued)

Compared with Fig. 4-3b, Fig.4-5b shows a big difference between the sample deposited at 10mTorr, 20°C and the one deposited at 10mTorr, 250°C. Unlike the former exhibiting a kind of stripe domain with strong contrast, the latter shows a unclear domain configuration like that obtained from the sample deposited at 5mTorr, 250°C. This matches the VSM results that the hysteresis loop obtained from the sample deposited at 10mTorr, 250°C behaves like that of the sample deposited at 5mTorr, 250°C, which exhibits a preferable in-plane magnetic anisotropy.

For the sample deposited at 20mTorr, 250°C, like the sample deposited at 20mTorr, 20°C, discontinuous domains without strong contrast appear.

For the samples deposited at 30 and 40mTorr, probably, due to the similar reasons for the samples deposited at 20°C, 30mTorr and 40mTorr, no domain information is observed.

4.2 Annealing Results

Subsequent annealing has been carried out in the chamber of the PLD system under a base pressure of 8×10^{-7} Torr and an annealing temperature of 200°C.

Annealing at 200°C did not make differences for the samples deposited at 10mTorr, 250°C and 20mTorr, 250°C. VSM measurements show that the annealing did not affect the hysteresis loops' shapes and the total magnetic moments. XRD measurements did not reveal differences in the phase structures. MFM results also find that there are no distinct differences before annealing and after annealing.

However, for the samples deposited at 10mTorr, 20°C and 40mTorr, 20°C, the annealing experiment affected the film properties. VSM measurements find that the hysteresis loops of these samples are varied.

Fig.4-6 compares the hysteresis loops determined from the sample deposited at 10mTorr, 20°C before annealing and after annealing.

The hysteresis loop obtained after annealing exhibits a behavior like that of the pure iron film, which shows that the annealed sample is much easier to saturate. This demonstrates that the perpendicular magnetic anisotropy was suppressed after annealing.

This can be understood by the explanation that the annealing process releases the stress, and thus decreases the stress-induced perpendicular anisotropy. XRD results taken from the sample before annealing and after annealing show that after annealing (shown in Figure 4-7), the tetragonal distortion of sample appears to be decreased. The α' peak appears lower and broader, but its center appears to have shifted to the right. (A new peak also shows up at about 38°, which has not been identified.) MFM images shown in Fig.4-8a and 8b also demonstrate this kind of stress change. After the post-deposition annealing process, the stripe domains with preferable orientation become less continuous and irregular. As stated above, stripe domains are closely related to the stress-induced perpendicular anisotropy. With the increase of the perpendicular anisotropy component, stripe domains have been observed to become coarsened and more regular [39, 40].

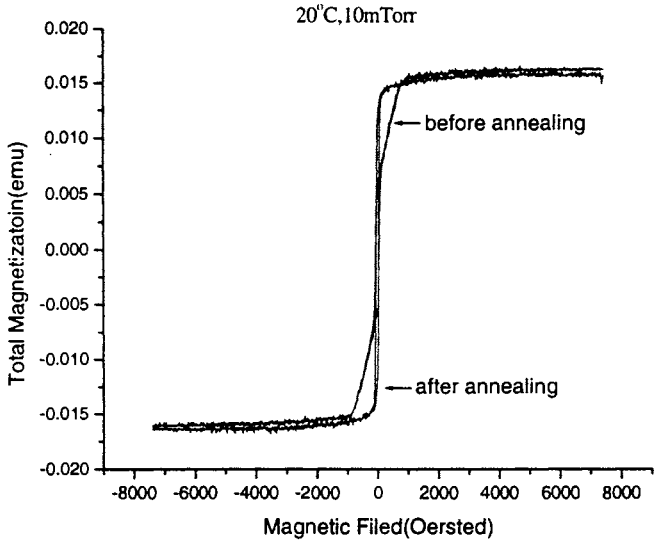

Figure 4-6 The hysteresis loops for the sample deposited at 10mTorr, 20°C before annealing and after annealing.

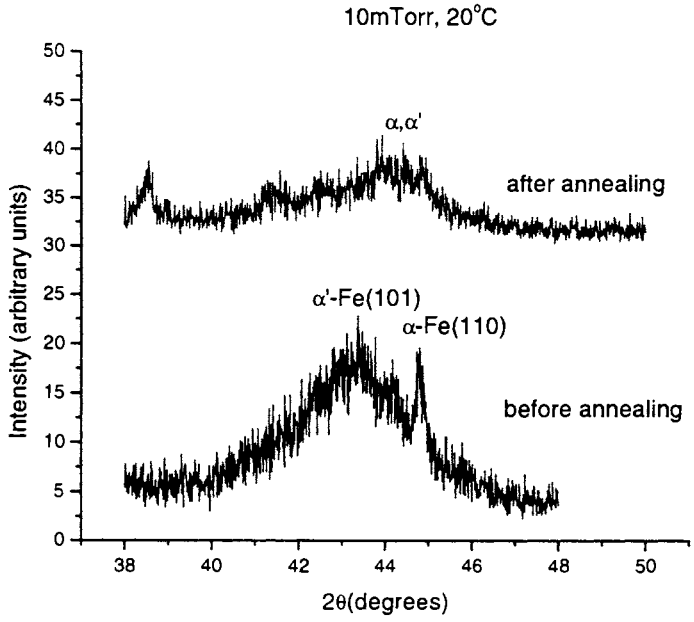

Figure 4-7 XRD obtained from the sample deposited at 10mTorr, 20oC before annealing and after annealing.

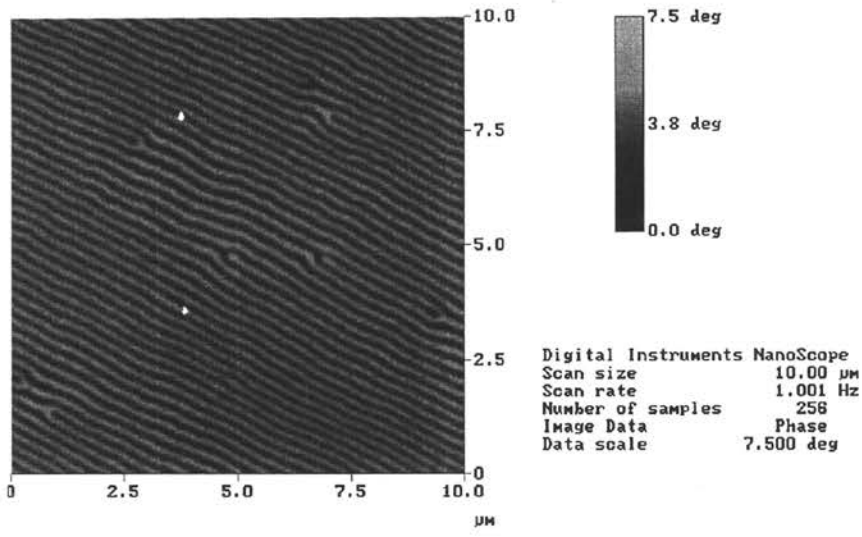

(a)

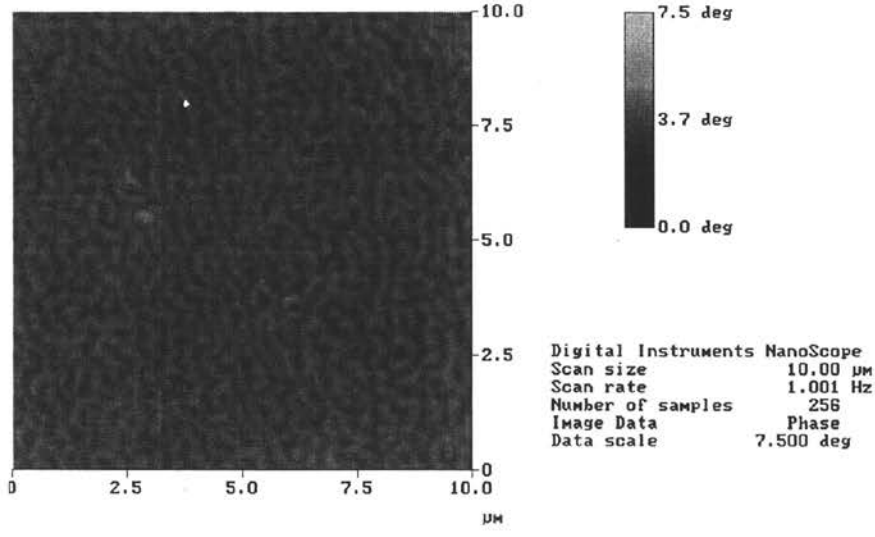

(b)

Figure 4-8 MFM images for the samples: a) as-deposited at 10mTorr, 20°C; b) after annealed at 200°C

The hysteresis loop's change for the sample deposited at 40mTorr, 20°C before annealing and after annealing is shown in Fig.4-9. For this sample, the magnetization decreased dramatically. It is found that the total magnetic moment obtained after annealing is almost a factor of 2 less that obtained before annealing. However, the XRD still shows no discernable peaks, which means that the sample is still amorphous or very fine nanograined after annealing. MFM results also did not show any changes.

Since there is a large saturation magnetization change but no phase change, it appears that short-range atomic order is changing. An amorphous structure lacks long-range atomic order. But the local atomic arrangement in amorphous structure is not completely random, and this kind of short-range order fundamentally affects the local atomic moment and the Curie temperature of the amorphous magnetic materials. The reason that the sample's magnetization decreased significantly may be explained as follows: an introduced annealing process could make the distribution of the nitrogen atoms more homogeneous (or ordered). N nearest neighbors are proposed to tend to decrease the moments on Fe atoms [9], and thus it is assumed that spreading the N more homogeneously causes more iron atoms to have N neighbors and thus overall moment decreases.

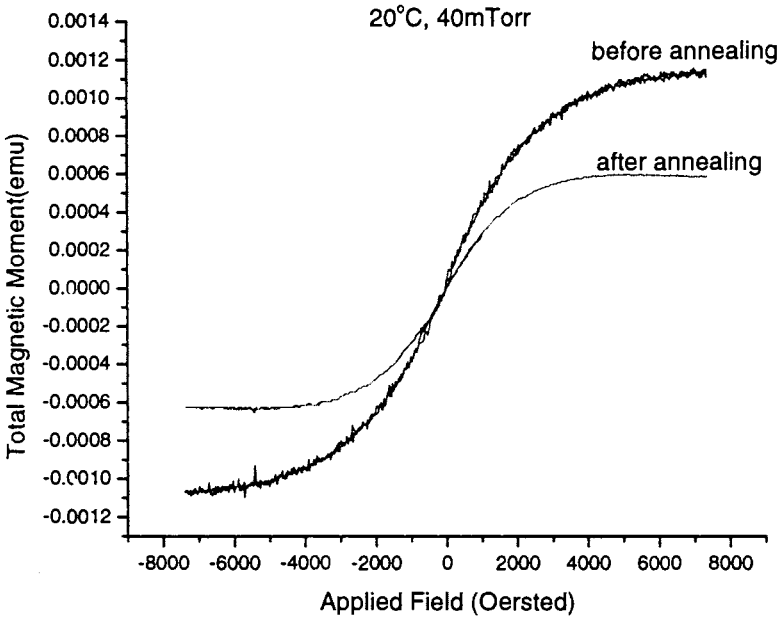

Figure 4-9 The hysteresis loops for the sample deposited at 40mTorr, 20°C before annealing and after annealing.

5. CONCLUSIONS

Fe-N films of a wide range of N contents were deposited on SiO_2/Si substrates at 20°C and 250°C by reactive pulsed laser deposition (PLD). Nitrogen pressure and substrate temperature play major roles in determining what structure (phase) and phase mixtures form. Film average nitrogen content plays an important role in influencing film average M_s, but in a multi-phase sample, its influence is somewhat indirect. Film average M_s is determined by which phases are present and their relative amounts and composition. The phase progression at 20°C substrate temperature is less like the bulk phase diagram than that at 250°C substrate temperature. This can be understood in terms of a model that takes into account the relative contributions of substrate temperature and deposition rate to a growing film. We did not observe the same phase mixtures as Yoshitake and Ohkoshi, particularly at 250°C. This could be due to major differences in the deposition rate between the two processes. To date, we have not observed M_s values greater than pure Fe for reactive PLD deposited Fe-N films. The bulk phase diagram, the Slater-Pauling curve and existing theoretical models do not predict enhanced magnetization values in the Fe-N system much above that of pure Fe [9]. Thus if they do exist in this system, large increases in magnetization must be connected with non-equilibrium structures/nanostructures formed by highly non-equilibrium processes.

Subsequent annealing at 200°C only shows changes for the samples deposited at 10mTorr and 40mTorr, 20°C. For the sample deposited 10mTorr, 20°C, it is found that the perpendicular magnetic anisotropy is suppressed after annealing. This can be understood by the explanation that the annealing process releases the stress. For the sample deposited at

40mTorr, 20°C, after annealing its magnetization is found to decrease significantly. The introduced annealing process is thought to make the distribution of the interstitial nitrogen atoms more homogeneous (or ordered). N nearest neighbors are proposed to tend to decrease the moments on Fe atoms, and thus it is assumed that spreading the N more homogeneously could cause more iron atoms have N neighbors and thus overall moment decrease.

REFERENCES

[1] T.K. Kim and M. Takahashi, Appl. Phys. Lett. 20, 492 (1972).

[2] M. Takahashi, Solid State Phys. 7, 483 (1972).

[3] Y. Sugita, H. Takahashi, M. Komuro and M. Igarashi, J. Appl. Phys. 79, 5576 (1996).

[4] J.M.D. Coey, Phys. World. 6, 25 (1993).

[5] J.M.D. Coey, J. Appl. Phys. 76, 6632 (1994).

[6] M.Takahashi, H. Shoji, H. Takahashi, T. Wakiyama, M. Kinoshita, and W. Ohta, IEEE Trans. Magn. 29, 3040 (1993).

[7] H.A. Wriedt, N. A. Gokcen and R. H. Nafziger, Bull. Alloy Phase Diagrams, 8, 355 (1987).

[8] M.Q. Huang, W. E. Wallace, S. Simaizu, S. G. Sankar, J. Magn. Magn. Mater. 135, 226 (1994).

[9] J. M. D. Coey and P. A. I. Smith, J. Magn. Magn. Mater. 200, 405 (1999).

[10] K. K. Shih, M. E. Re and D. B. Dove, Appl. Phys. Lett. 57, 412 (1990).

[11] R. Hübler, S. R. Teixeira, W. H. Schreiner and I. J. R. Baumvol, Nuclear Instruments and Methods in Physics Research. B80/81, 1392 (1993).

[12] M. Komuto, Y. Kozono, M. Hanazono and Y. Sugita, J. Appl. Phys. 67, 5126 (1990).

[13] K. Nakajima and S. Okamoto, Appl. Phy. Lett. 54, 2536 (1989).

[14] S. Okamoto, O. Kitakami, and Y. Shimada, J. Appl. Phys. 79, 5250 (1996).

[15] S. Okamoto, O. Kitakami and Y. Shimada, J. of Appl. Phy. 85, 4952 (1999).

[16] H. Jiang, K. Tao, H. Li, J. Phys.: Condens. Matter. 6, L279 (1994).

[17] X.Z. Ding, F.M. Zhang, J.S. Yan, H.L. Shen, X. Wang, X.H. Liu, D.F. Shen, J. Appl. Phys. 82, 5154 (1997).

[18] M. Takahashi and H. Shoji, J. of Magn. and Magn. Mate. 208, 145 (2000).

[19] J. M. Cadogan, Aust. J. Phys. 50, 1093 (1997).

[20] J. M. D. Coey, K. O'Donnell, Q. Qi, E. Touchais, and K. H. Jack, J. Phys: Condens. Matter. 6, L23 (1994).

[21] A. Sakuma, J. Magn. Magn. Mater. 102, 127 (1991).

[22] T. Yoshitake and M. Ohkoshi, IEEE Trans. on Magn. 31, 3850 (1995).

[23] Douglas B.Chrisey and Graham K. Hubler, *Pulsed Laser Deposition of Thin Films*, (John Wiley& Sons, Inc., New York, 1994), pp. 23-54.

[24] P. K. Singh, D. Kumar, Mater. Sci. and Eng. R22, 113 (1998).

[25] *Introduction Manual for Model 4500 VSM*, (EG&G Princeton Applied Research Corporation, Princeton, 1992), pp. 5-7.

[26] PerkinElmer Instruments, *What is a lock-in Amplifier*, http://www.optics.arizona.edu/Palmer/opti470a/PDF/tn1000.pdf, 11/25/2002.

[27] B. J. Hunt and I. James, *Polymer Characterization*, (Blackie Academic and Professional, New York, 1993), pp. 121-123

[28] B.D.Cullity, *Elements of X-ray Diffraction*, (Addison-Wesley Publishing Company, Inc., Reading, Massachusetts, 1978), pp. 81-143.

[29] *Scanning Probe Microscopy Training Notebook*, (Digital Instruments, Veeco Metrology Group, Santa Barbara, 1998), pp. 8

[30] R. C. Weast, Ed, Handbook of Chemistry and Physics (The Chemical Rubber Co.

Cleveland, OH, 1971), pp.D-65.

[31] J. Zhou, D. Li, Y. Gu, X. Chang, C. Zhao, F. Li and L. Qiao, IEEE Trans. Magn. 37, 3844 (2001).

[32] H.A. Wriedt, N. A. Gokcen and R. H. Nafziger, Bull. Alloy Phase Diagrams, 8, 355 (1987).

[33] L. Luo, B. Yao, H. Wang, F. Li, B. Ding, and W. Su, J. Non-Cryst. Solids. 277, 91 (2000).

[34] T. Hioko and M. Ohkubo, Toyota Chuo Kenkyusho R&D Rebyu. 22, 33 (1987).

[35] H. D. Luc and V. H. Lam, Commun. Phys. (Hanoi) 5, 34 (1995).

[36] M. Gupta, A. Gupta, S. M. Chaudhari, D. M. Phase, V. Ganesan, M. V. R. Rao, T. Shripathi, and B. A. Dasannacharya, Vacuum. 60, 395 (2001).

[37] E. Y. Jiang, D. C. Sun, H. Liu, H. L. Bai, and X. X. Zhang, J. Magn. Magn. Mater. 140, 719 (1995).

[38] N. Saito, H. Fujiwara, and Y.Sugita, J. Phys. Soc. Jpn. 19, 1116 (1964).

[39] C. C. H. Lo, J. E. Snyder, J. Leib, R. Chen, B. Kriegermeier-Sutton, M. J. Kramer, D. C. Jiles, and M.T. Kief. J. Appl. Phys. 89, 2868 (2001).

[40] J. E. Snyder, C. C. H. Lo, R. Chen, B. Kriegermeier-Sutton, J. Leib, S. J. Lee, M. J. Kramer, D.C. Jiles and M. T. Kief. J. Magn. Magn. Mater. 226-230, 1669 (2001).